Available online at www.sciencedirect.com
SCIENCE DIRECT®
Journal of the European Ceramic Society 25 (2005) 313–333
www.elsevier.com/locate/jeurceramsoc

Critical thermodynamic evaluation and optimization of the CaO–MgO–SiO_2 system

In-Ho Jung, Sergei A. Decterov, Arthur D. Pelton*

Centre de Recherche en Calcul Thermochimique (CRCT), École Polytechnique de Montréal, P.O. Box 6079, Station "Downtown", Montréal, Que., Canada H3C 3A7

Received 24 November 2003; accepted 8 February 2004
Available online 2 June 2004

Abstract

A complete literature review, critical evaluation and thermodynamic modeling of phase diagrams and thermodynamic properties of all oxide phases in the CaO–MgO–SiO_2 system at 1 bar pressure are presented. The molten oxide phase is described by the Modified Quasichemical Model, and the Gibbs energies of the olivine and pyroxene solid solutions are modeled using the compound energy formalism. A set of optimized model parameters of all phases is obtained which reproduces all available and reliable thermodynamic and phase-equilibrium data within experimental error limits from 25 °C to above the liquidus temperatures over the entire composition range. The complex phase relationships in the system have been elucidated, and discrepancies among the data have been resolved. The database of the model parameters can be used along with software for Gibbs energy minimization in order to calculate all thermodynamic properties and any phase diagram section or phase equilibrium of interest.

Keywords: Phase equilibrium; CaO–MgO–SiO_2; Phase diagrams; Refractories; Thermodynamic modeling

1. Introduction

The CaO–MgO–SiO_2 system is of great importance in metallurgy and geochemistry. The phase equilibria, thermodynamic properties of solid and liquid phases and structural properties of solid solutions have been widely investigated at 1 bar and also at high pressure. The purpose of this study is to critically evaluate and optimize all available experimental data at 1 bar pressure.

In a thermodynamic "optimization" of a system, all available thermodynamic and phase-equilibrium data are evaluated simultaneously in order to obtain one set of model equations for the Gibbs energies of all phases as functions of temperature and composition. From these equations, all of the thermodynamic properties and the phase diagrams can be back-calculated. In this way, all the data are rendered self-consistent and consistent with thermodynamic principles. Thermodynamic property data, such as activity data, can aid in the evaluation of the phase diagram, and phase diagram measurements can be used to deduce thermodynamic properties. Discrepancies in the available data can often be resolved, and interpolations and extrapolations can be made in a thermodynamically correct manner. A small set of model parameters is obtained. This is ideal for computer storage and calculation of properties and phase diagrams.

Thermodynamic optimizations for this system have already been reported by Pelton and Eriksson[1] using simple solid solution models and the Modified Quasichemical Model[2–5] for the liquid oxide, and by Huang et al.[6] who used the two-sublattice compound energy formalism[7] for the solid solutions and the ionic liquid model[8] for the liquid oxide. However, several important experimental studies of thermodynamic properties and phase equilibria have been performed subsequently. A wider range of experimental data, including structural information on solid solutions such as olivine, has been collected, evaluated and optimized in the course of the present study, and a better overall description of all the experimental data was obtained compared to the previous optimizations.

The binary sub-systems, CaO–MgO,[9] CaO–SiO_2[10] and MgO–SiO_2[11] have already been optimized and the opti-

* Corresponding author. Tel.: +1-514-340-4711x4531; fax: +1-514-340-5840.
E-mail address: arthur.pelton@polymtl.ca (A.D. Pelton).

0955-2219/$ – see front matter © 2004 Elsevier Ltd. All rights reserved.
doi:10.1016/j.jeurceramsoc.2004.02.012

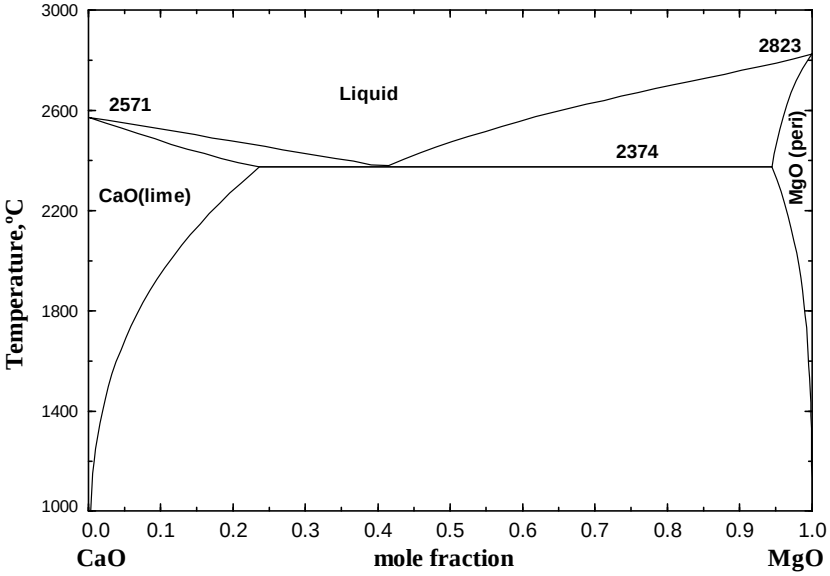

Fig. 1. Calculated CaO–MgO phase diagram.[9]

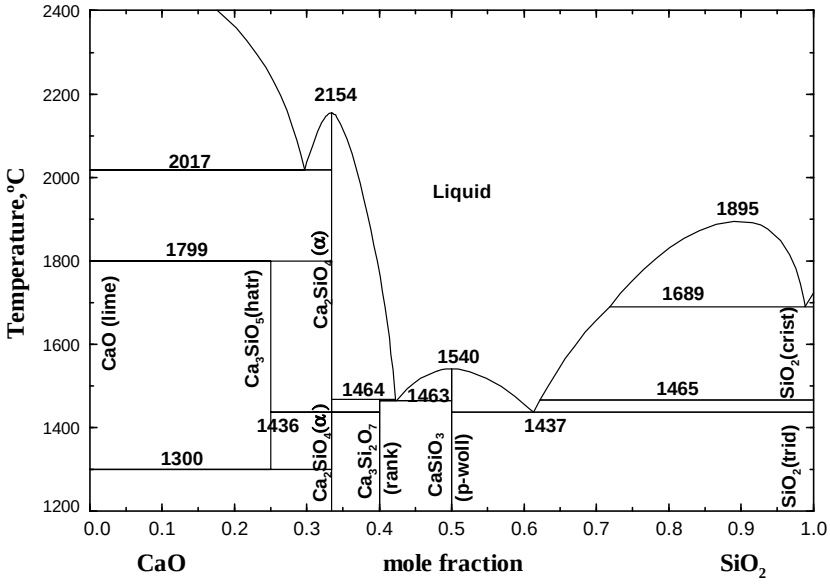

Fig. 2. Calculated CaO–SiO_2 phase diagram.[10]

mized binary model parameters are used without change in the present study. Phase diagrams calculated from the optimized parameters are shown in Figs. 1–3. In the evaluations/optimizations, all available phase diagram data from several sources, metastable phase-equilibrium data, data on the Gibbs energies of all compounds, and measured activities of SiO_2 in the CaO–SiO_2 and MgO–SiO_2 slags were simultaneously taken into account. The optimized binary model parameters for the Modified Quasichemical Model for the liquid phase as well as optimized expressions for the Gibbs energies of all compounds and for the CaO–MgO solid solution are given in Wu et al.[9,11] and Eriksson et al.[10] Based on these binary assessments, the CaO–MgO–SiO_2 system is optimized in the present study. The resultant model database provides the best presently available description of the thermodynamic properties and phase equilibria.

2. Thermodynamic models

All compounds and solutions are summarized in Table 1 to clarify the names of the minerals and solutions used in this study. All optimized model parameters are listed in Table 2.

2.1. Molten oxide (slag)

For the molten oxide (slag) phase, the Modified Quasichemical Model[2,3] has been used. This model has

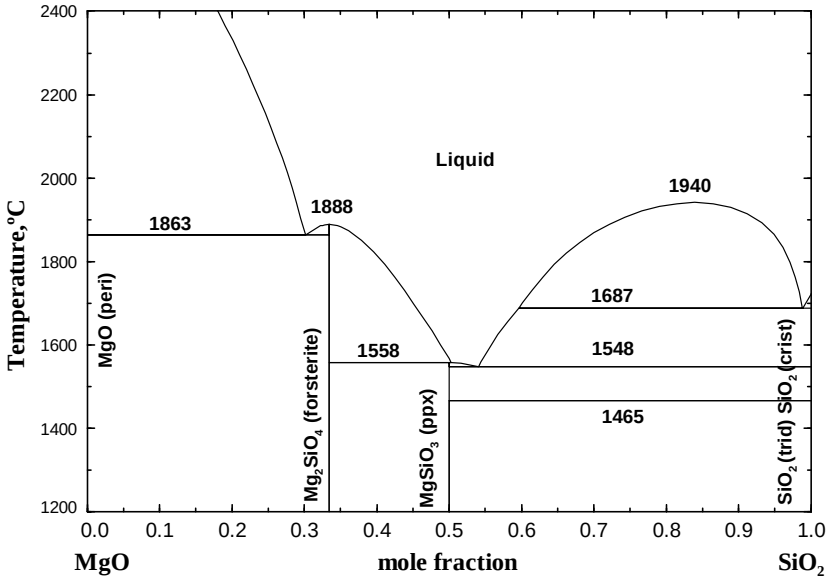

Fig. 3. Calculated MgO–SiO_2 phase diagram.[11]

been recently further developed and summarized.[4,5] Short-range ordering is taken into account by considering second-nearest-neighbor pair exchange reactions. For example, for the CaO–MgO–SiO_2 slags these reactions are:

$$(\text{Ca–Ca}) + (\text{Si–Si}) = 2(\text{Ca–Si}), \quad \Delta g_{\text{CaO, SiO}_2} \tag{1}$$

$$(\text{Mg–Mg}) + (\text{Si–Si}) = 2(\text{Mg–Si}), \quad \Delta g_{\text{MgO, SiO}_2} \tag{2}$$

$$(\text{Ca–Ca}) + (\text{Mg–Mg}) = 2(\text{Ca–Mg}), \quad \Delta g_{\text{CaO, MgO}} \tag{3}$$

where (A–B) represents a second-nearest-neighbor A–B pair. The parameters of the model are the Gibbs energies $\Delta g_{\text{A, B}}$ of these reactions, which may be expanded as empirical functions of composition.

The optimized binary model parameters as well as the optimized expressions for the Gibbs energies of all stoichiometric compounds are given in Wu et al.[9,11] and Eriksson et al.[10] along with the second-nearest-neighbor "coordination numbers" of Ca, Mg and Si used in the Modified Quasichemical Model. The asymmetric "Toop-like"[12] extension of binary model parameters is used in order to calculate the Gibbs energy of the ternary liquid, with SiO_2 as the "asymmetric component". In order to reproduce the ternary phase diagram of the CaO–MgO–SiO_2 system, three small opti-

Table 1
Names of all solid and liquid phases in the CaO–MgO–SiO_2 system at 1 bar pressure

Phase name	Formula	Other names
Olivine	$(Ca^{2+},Mg^{2+})(Ca^{2+},Mg^{2+})SiO_4$	Forsterite (Fors): Mg_2SiO_4 rich olivine Monticellite (Mont): $CaMgSiO_4$ rich olivine γ-Ca_2SiO_4 (γ): Ca_2SiO_4 rich olivine
Clino-pyroxene (cpx) (monoclinic, C2/c)	$(Ca^{2+},Mg^{2+})(Mg^{2+})Si_2O_6$	Diopside (Diop): $CaMgSi_2O_6$ rich clino-pyroxene Pigeonite (Pig): $MgSiO_3$ rich clino-pyroxene
Ortho-pyroxene (opx) (orthorhombic, Pbca)	$(Ca^{2+},Mg^{2+})(Mg^{2+})Si_2O_6$	Ortho-enstatite ($MgSiO_3$ rich ortho-pyroxene)
Proto-pyroxene (ppx) (orthorhombic, Pbcn)	$(Ca^{2+},Mg^{2+})(Mg^{2+})Si_2O_6$	Proto-enstatite ($MgSiO_3$ rich proto-pyroxene)
Low clino-pyroxene (monoclinic, P21/c)	$(Ca^{2+},Mg^{2+})(Mg^{2+})Si_2O_6$	Low clino-enstatite ($MgSiO_3$ rich low clino-pyroxene)
Monoxide	$(Ca^{2+},Mg^{2+})O$	Lime (CaO): CaO rich monoxide Periclase (MgO): MgO rich monoxide
Wollastonite (Woll)	$(Ca^{2+},Mg^{2+})SiO_3$	
α′-Ca_2SiO_4 (α′)	$(Ca^{2+},Mg^{2+})_2SiO_4$	
α-Ca_2SiO_4 (α)	$(Ca^{2+},Mg^{2+})_2SiO_4$	
Molten oxide (L)	CaO–MgO–SiO_2	Slag
Akermanite (Aker)	$Ca_2MgSi_2O_7$	
Merwinite (Merw)	$Ca_3MgSi_2O_8$	
Pseudo-wollastonite (P-Woll)	$CaSiO_3$	
Silica	SiO_2	Quartz, tridymite (Trid), cristobalite (Crist)
Hatrurite (Hatr)	Ca_3SiO_5	
Rankinite (Rank)	$Ca_3Si_2O_7$	

Table 2
Optimized model parameters of solutions and compounds in the CaO–MgO–SiO_2 system (J/mol)

Olivine: $(Ca^{2+},Mg^{2+})^{M2}(Ca^{2+},Mg^{2+})^{M1}SiO_4$
$G_{MgMg} = G^{\circ}(Mg_2SiO_4)$[35]
$G_{CaCa} = G^{\circ}(Ca_2SiO_4)$[35]
$G_{CaMg} = G^{\circ}(CaMgSiO_4$[18]$) - 3345$
$G_{MgCa} = G_{CaMg} + 146440$
${}^0L_{CaMg:Ca} = {}^0L_{CaMg:Mg} = 32235.53$
${}^1L_{CaMg:Ca} = {}^1L_{CaMg:Mg} = 4279.92$
${}^0L_{Ca:CaMg} = {}^0L_{Mg:CaMg} = 28032.8 - 12.55T$

Pyroxene: $(Ca^{2+},Mg^{2+})^{M2}(Mg^{2+})^{M1}Si_2O_6$
$G^{\circ}(MgSiO_3$, low clino-), $G^{\circ}(MgSiO_3$, proto-), $G^{\circ}(MgSiO_3$, ortho-) from F*A*C*T.[35]
$G^{\circ}(MgSiO_3$, clino-$) = G^{\circ}(MgSiO_3$, low clino-$) + 4694.5 - 3.70T$
$G^{\circ}(CaMgSi_2O_6$, clino-$) = G^{\circ}$(clino-$CaMgSi_2O_6$[18]$) + 837$
$G^{\circ}(CaMgSi_2O_6$, low clino-$) = G^{\circ}(CaMgSi_2O_6$, clino-$) + 28368$
$G^{\circ}(CaMgSi_2O_6$, ortho-$) = G^{\circ}(CaMgSi_2O_6$, clino-$) + 19740 + 0.02T$
$G^{\circ}(CaMgSi_2O_6$, proto-$) = G^{\circ}(CaMgSi_2O_6$, clino-$) + 17071.2$
Low clino-pyroxene: ${}^0L_{CaMg:Mg} = 25304.0 + 2.358T$
Ortho-pyroxene: ${}^0L_{CaMg:Mg} = 27247.8 - 8.622T$
Proto-pyroxene: ${}^0L_{CaMg:Mg} = 25304.0 + 2.358T$
Clino-pyroxene: ${}^0L_{CaMg:Mg} = 25304.0 + 2.358T$,
${}^1L_{CaMg:Mg} = -3018.6$

Wollastonite: $(Ca^{2+},Mg^{2+})SiO_3$
$G^{\circ}(MgSiO_3) = G^{\circ}(MgSiO_3$, ortho-pyroxene$) + 48987.6 - 17.145T$

α-Ca_2SiO_4: $(Ca^{2+},Mg^{2+})_2SiO_4$
$G^{\circ}(\alpha\text{-}Mg_2SiO_4) = G^{\circ}(Mg_2SiO_4$, olivine$) + 83680.0$
$q^{03}_{MgCa} = -35564$

α′-Ca_2SiO_4: $(Ca^{2+},Mg^{2+})_2SiO_4$
$G^{\circ}(\alpha'\text{-}Mg_2SiO_4) = G^{\circ}(Mg_2SiO_4$, olivine$) + 85772$
$q^{03}_{MgCa} = -35564$

Liquid oxide: CaO–MgO–SiO_2
$q^{001}_{MgO,SiO_2(CaO)} = 4184$
$q^{001}_{CaO,SiO_2(MgO)} = 8368$
$q^{021}_{CaO,SiO_2(MgO)} = -29288$

The quasichemical parameters are defined in Pelton et al.[4] The other binary model parameters for the liquid oxide can be found in the previous studies.[9–11] Thermodynamic properties ($S_{298.15}$, $H_{298.15}$, C_P) of $CaMgSiO_4$, clino-$CaMgSi_2O_6$, $Ca_2MgSi_2O_7$ and $Ca_3MgSi_2O_8$ were taken from Berman[18] with the enthalpies of formation at 298.15 K changed by −3345, 837, −5850 and −18280 J/mol, respectively. The Gibbs energies of the other end-members of the solid and liquid solutions and of the other stoichiometric compounds in the CaO–MgO–SiO_2 system are taken from the F*A*C*T database[35] and previous studies.[9–11] The binary model parameters for the monoxide and liquid oxide solutions are given in the previous studies.[9–11]

mized ternary model parameters were added in the present study. These are listed in Table 2.

2.2. Olivine solid solution

The olivine solid solution has two distinct octahedral sublattices, called M2 and M1:[13–15]

$$(Ca^{2+}, Mg^{2+})^{M2}(Ca^{2+}, Mg^{2+})^{M1}SiO_4 \quad (4)$$

where cations shown within a set of brackets occupy the same sublattice.

Because the M2 sites are bigger than M1 sites, Ca^{2+} preferentially enters the M2 sites. Monticellite, $CaMgSiO_4$, is part of the olivine solution. For the olivine solution, the model is developed within the framework of the compound energy formalism (CEF).[7] The Gibbs energy expression in the CEF per formula unit of a solution is as follows:

$$G = \sum_i \sum_j Y_i^{M2} Y_j^{M1} G_{ij} - TS_C + G^E \quad (5)$$

where Y_i^{M2} and Y_j^{M1} represent the site fractions of constituents i and j on the M2 and M1 sublattices, G_{ij} is the Gibbs energy of an "end-member" $(i)^{M2}(j)^{M1}SiO_4$, in which the M2 and M1 sublattices are occupied only by i and j cations, respectively, S_C is the configurational entropy assuming random mixing on each sublattice given by:

$$S_C = -R\left(\sum_i Y_i^{M2} \ln Y_i^{M2} + \sum_j Y_j^{M1} \ln Y_j^{M1}\right) \quad (6)$$

and G^E is the excess Gibbs energy given by:

$$G^E = \sum_i \sum_j \sum_k Y_i^{M2} Y_j^{M2} Y_k^{M1} L_{ij:k} + \sum_i \sum_j \sum_k Y_k^{M2} Y_i^{M1} Y_j^{M1} L_{k:ij} \quad (7)$$

where $L_{ij:k}$ and $L_{k:ij}$ are interaction energies between cations i and j on one sublattice when the other sublattice is occupied by k. The dependence of the interaction energies on composition can be expressed by Redlich–Kister power series:

$$L_{ij:k} = \sum_m^m L_{ij:k}(Y_j^{M2} - Y_i^{M2})^m \quad (8)$$

$$L_{ij:k} = \sum_m^m L_{k:ij}(Y_j^{M1} - Y_i^{M1})^m \quad (9)$$

Optimized model parameters are listed in Table 2.

2.3. Pyroxene solid solution

There are four pyroxene solutions with different crystal structures: ortho-, proto-, clino-, and low clino-. Like olivine, the pyroxenes have two distinct octahedral sublattices, M2 and M1.[15–17] However, unlike olivine, the amount of Ca on the M1 sites is negligibly small, so that the formula unit of pyroxenes can be written as

$$(Ca^{2+}, Mg^{2+})^{M2}(Mg^{2+})^{M1}Si_2O_6 \quad (10)$$

In the CaO–MgO–SiO_2 system, the end-members of the pyroxene solutions are $Mg_2Si_2O_6$ and $CaMgSi_2O_6$, and the mixing of cations occurs only on the M2 sites. The Gibbs energy of a pyroxene solution is expressed using Eq. (5) of the compound energy formalism. Optimized model parameters are listed in Table 2.

2.4. Wollastonite, α-Ca_2SiO_4 and α′-Ca_2SiO_4 solid solutions

Magnesium can substitute for calcium in wollastonite, $CaSiO_3$, which has a silicate chain structure and in α- and α′-Ca_2SiO_4. A simple random mixing model with a polynomial expansion of the excess Gibbs energy is used for these solutions:

$$G = (G^{\circ}_{A}X_A + G^{\circ}_{B}X_B) + nRT(X_A \ln X_A + X_B \ln X_B) + G^{E} \quad (11)$$

$$G^{E} = \sum q^{ij}_{AB}(X_A)^i(X_B)^j \quad (12)$$

where G is the Gibbs energy per formula unit of a solution (see Table 1), G°_{A} and G°_{B} are the Gibbs energies of the pure end-members, G^{E} is the excess Gibbs energy, X_A and X_B are mole fractions of end-members, q^{ij}_{AB} are the model parameters, and $n = 1$ for wollastonite and $n = 2$ for the α- and α′-Ca_2SiO_4 solutions. Optimized model parameters are listed in Table 2.

2.5. Monoxide solid solution

The monoxide solid solution exists in the CaO–MgO binary system (see Fig. 1). MgO and CaO have limited solubilities in each other forming a solid miscibility gap. The model parameters were taken from the previous study by Wu et al.[9]

2.6. Stoichiometric compounds

Pseudowollastonite ($CaSiO_3$), hatrurite (Ca_3SiO_5), rankinite ($Ca_3Si_2O_7$), SiO_2, akermanite ($Ca_2MgSi_2O_7$) and merwinite ($Ca_3MgSi_2O_8$) are considered to be stoichiometric compounds in this study.

3. Evaluation/optimization of experimental data

The liquidus surface calculated from the optimized parameters is shown in Fig. 4. Along the orthosilicate and metasilicate sections, extensive solid solutions such as olivine and pyroxenes exist. The other solid solutions such as wollastonite, α- and α′-Ca_2SiO_4 exhibit limited solubility. All calculated invariant points involving the liquid oxide are given in Table 3. The details of various phase diagram sections will be discussed in the following. The Gibbs energies of the akermanite, diopside, merwinite and monticellite ternary compounds were taken from the assessment by Berman,[18] with small corrections being made to the enthalpies of formation, $H^{\circ}_{298.15}$ as shown in Table 2 in order to reproduce the phase diagram data.

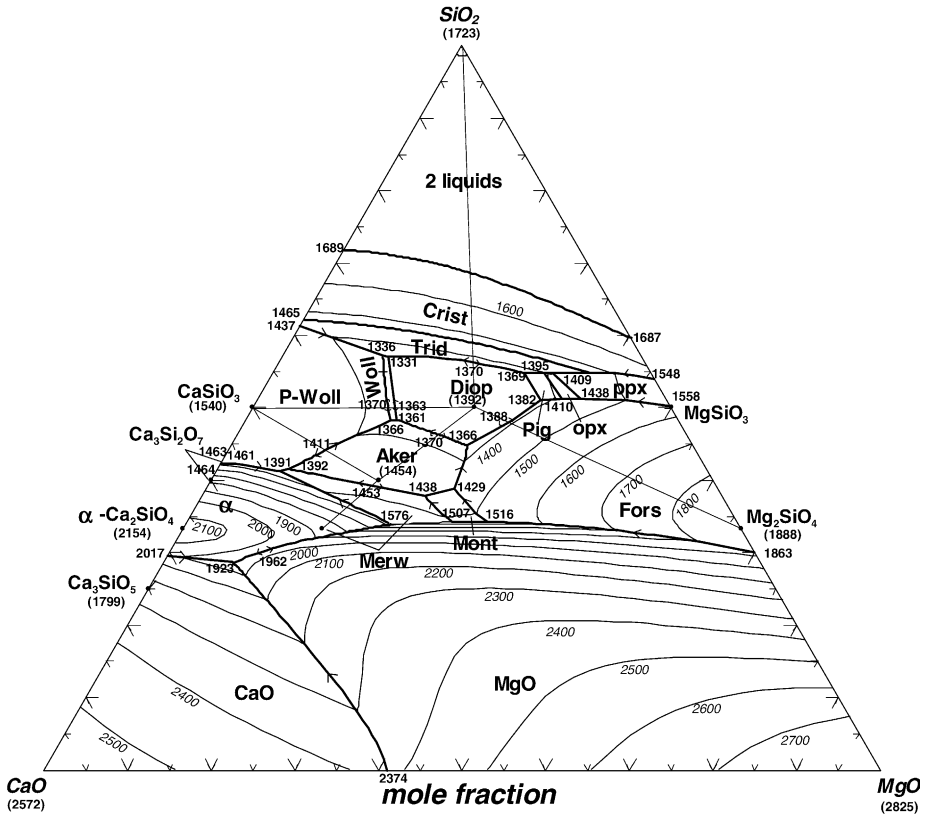

Fig. 4. Calculated (optimized) liquidus surface of the CaO–MgO–SiO_2 system at 1 bar pressure. Temperatures in degree Celsius. See Table 1 for abbreviations of phase names.

Table 3
Comparison of the calculated and experimental ternary invariant points involving liquid oxide in the CaO–MgO–SiO_2 system

Invariant point[a]	T (°C)		Liquid composition (mol%)						Reference
	Calc.	Exp.	CaO		MgO		SiO_2		
			Calc.	Exp.	Calc.	Exp.	Calc.	Exp.	
L → CaO + MgO + α	1923		63.0		8.4		28.6		
L + MgO + α → Merw	1576	1575	41.5	41.1	24.6	24.3	33.9	34.6	21
L + MgO + Merw → Mont	1507		34.1		31.6		34.3		
L + MgO + Fors → Mont	1516	1502	29.8	29.8	35.9	34.2	34.3	36.0	22
L + Merw + Mont → Aker	1438	1436	35.5	37.4	26.6	24.4	37.9	38.2	28
L + Mont + Fors → Aker	1429	1430	31.4	31.5	29.7	29.3	38.9	39.2	28
L + Merw + Aker → P-woll	1392		49.7		8.8		41.5		
L → α + Merw + P-woll	1391		51.2		7.6		41.2		
L + Rank → α + P-woll	1461		56.5		1.5		42.0		
L → Aker + Diop + Fors	1366	1357	27.0	26.9	28.2	28.5	44.8	44.6	28
L → Aker + Diop + Woll	1361	1350	33.7	35.1	18.0	17.5	48.3	47.4	53
L + Aker + P-woll → Woll	1366	1360	34.4	36.4	17.3	16.2	48.3	47.4	53
L + Tridy + P-woll → Woll	1336	1336	31.0	32.0	12.0	9.5	57.0	58.5	53
L → Woll + Tridy + Diop	1331	1320	30.3	30.8	12.6	11.2	57.1	58.0	53
L + Fors + ppx → opx	1438	1445	10.1	11.7	38.6	35.8	51.3	52.5	43
L + Fors + opx → Pige	1410	1410	12.4	14.8	36.3	32.7	51.3	52.5	43
L + Fors → Diop + Pige	1382	1385	15.1	17.0	33.9	31.0	51.0	52.0	43
L + ppx + Tridy → opx	1409	1419	11.7	12.7	33.4	31.0	54.9	56.3	43
L + opx + Tridy → Pige	1395	1387	12.8	15.0	32.4	28.4	54.8	56.6	43
L → Pige + Diop + Tridy	1369	1373	15.1	16.4	30.1	27.5	54.8	56.1	43

[a] The ambiguous invariant points involving hatrurite (Ca_3SiO_5) and rankinite ($Ca_3Si_2O_7$) estimated by Ricker and Osborn[24] and Osborn[23] are not included in the table (see text for details).

3.1. Orthosilicate section

Fig. 5 shows the calculated phase diagram of the Ca_2SiO_4–Mg_2SiO_4 section. γ-Ca_2SiO_4, monticellite and forsterite all belong to the olivine solution. Between monticellite and forsterite, the olivine solution is known to exhibit a miscibility gap. MgO dissolving a small amount of CaO appears as a primary crystalline phase in the middle of the phase diagram.

Gutt[19] measured the phase diagram over the composition region between Ca_2SiO_4 and merwinite from 25 °C to liquidus temperatures. His results are shown on Fig. 6. Liquidus temperatures between 1800 and 2130 °C were measured by high-temperature microscopy. The subsolidus regions were

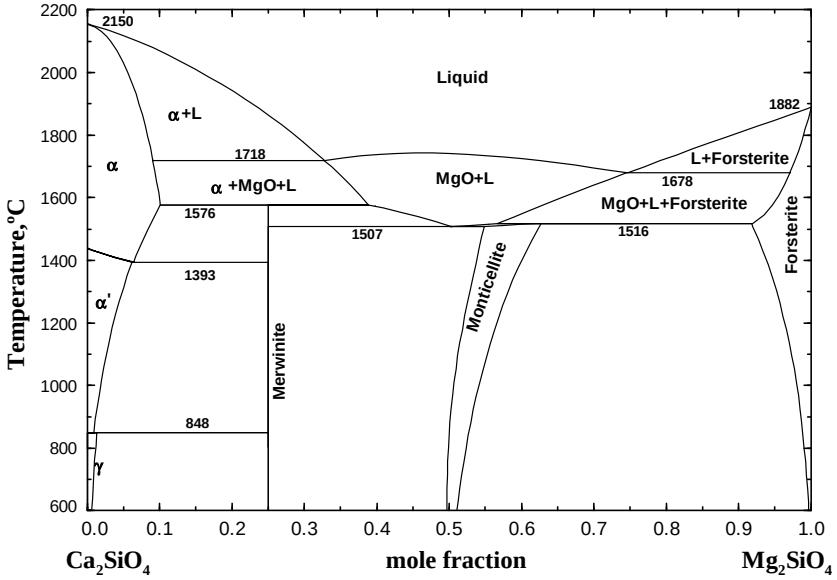

Fig. 5. Calculated phase diagram of the Ca_2SiO_4–Mg_2SiO_4 orthosilicate section.

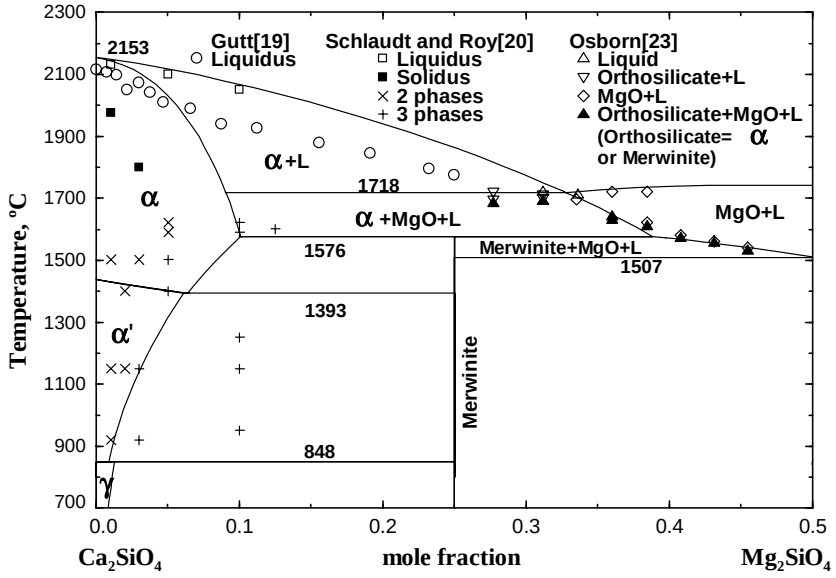

Fig. 6. Calculated phase diagram of the Ca_2SiO_4–$CaMgSiO_4$ section.

studied systematically by high-temperature X-ray analysis up to 1575 °C, and quenching in combination with X-ray analysis was used between 1575 and 1590 °C. Gutt found very limited solubility of Mg^{2+} in α′- and γ-Ca_2SiO_4, and no solubility in α-Ca_2SiO_4. Phase transitions from α to α′ and from α′ to γ-Ca_2SiO_4 were reported at 1360 and 990 °C, respectively. The so called "*T*" phase, $Ca_{1.7}Mg_{0.3}SiO_4$, was found to be stable up to 1460 °C and to decompose to α-Ca_2SiO_4 and merwinite. However, the topology of the phase diagram constructed by Gutt[19] is incorrect.

Schlaudt and Roy[20] studied the Ca_2SiO_4-monticellite join at temperatures up to 1600 °C using a standard quenching technique followed by microscopic and X-ray analysis (see Fig. 6). For temperatures higher than 1600 °C, a platinum or iridium strip furnace was used and temperatures were determined by an optical pyrometer. High-temperature DTA and high-temperature X-ray diffraction were used to study the α′ to α transition in Ca_2SiO_4, which was found to occur at 1400 °C. X-ray diffraction was shown to be unsuitable for determination of the solubility of Mg^{2+} in Ca_2SiO_4 because the shifts in the diffraction peaks with additions of magnesium were less than the experimental uncertainty. (This might explain the underestimated magnesium solubility in Ca_2SiO_4 reported by Gutt.[19]) Therefore, the phase boundaries of the Ca_2SiO_4 solid solutions were determined by the first appearance of phases other than Ca_2SiO_4. Merwinite was found to melt incongruently at 1575 °C to form Ca_2SiO_4, MgO and liquid. The "*T*" phase was observed in the temperature range from 979 to 1381 °C when gel starting materials were used. However, when crystalline oxide starting materials were used, this phase was not found. Schlaudt and Roy[20] reported very limited solubility of monticellite in merwinite. Sharp et al.[21] also observed a small solubility from electron microprobe analysis of merwinite samples equilibrated at about 5–10 kbar by Yoder.[22] The molar Mg/(Ca + Mg) ratio in merwinite varied from 0.25 to 0.26 (0.25 corresponds to stoichiometric merwinite), but the (Ca + Mg)/Si ratio was equal to 2 indicating that the merwinite solution exists only along the Ca_2SiO_4–Mg_2SiO_4 orthosilicate join. In the present study the limited homogeneity range of merwinite is ignored; i.e. merwinite is considered to be a stoichiometric compound.

Osborn[23] investigated phase relations in the merwinite–monticellite region using a quenching technique followed by microscopic phase determination (see Fig. 6). Merwinite was found to melt incongruently to MgO, Ca_2SiO_4 and liquid at 1575 °C. The liquidus of MgO was measured above 1700 °C.

Ricker and Osborn[24] investigated the monticellite–forsterite part of the orthosilicate section from 1100 to 1750 °C using a quenching technique followed by optical and X-ray phase analysis (see Fig. 7). Maximum solubilities of 30 wt.% monticellite in forsterite and of 30 wt.% forsterite in monticellite were observed at 1500 °C.

The olivine miscibility gap was investigated more thoroughly in several studies.[25–29] Biggar and O'Hara[26] studied subsolidus phase equilibria between monticellite and forsterite from 1200 to 1490 °C by the quenching technique using both gel and crystalline precursors in combination with optical and X-ray analysis. Yang[25] used EPMA of quenched samples to obtain the compositions of coexisting forsterite and monticellite solid solutions over the temperature range between 1440 and 1496 °C. Hatfield et al.[28] used the quenching method and microscopic analysis to measure the compatibility triangles among MgO solid solution, olivine and liquid oxide at 1550 and 1700 °C. The phase boundary of the forsterite solid solution obtained from these triangles substantiates the data of Biggar and O'Hara[26] and Yang.[25] The high pressure experiments by Warner and Luth[29] and by Adams and Bishop[27] also confirmed that the miscibility gap reported by Ricker and Osborn[24] is too narrow.

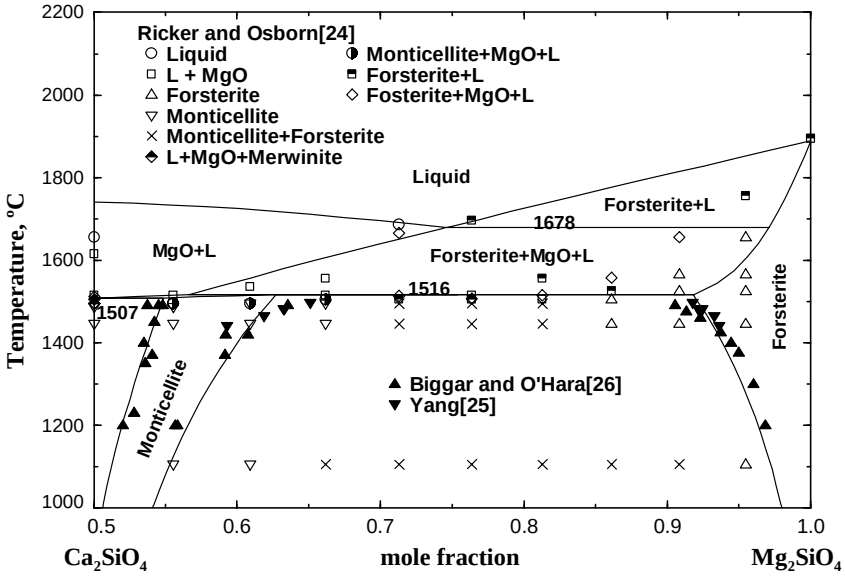

Fig. 7. Calculated phase diagram of the $CaMgSiO_4$–Mg_2SiO_4 section.

Monticellite ($CaMgSiO_4$) is often considered to be a stoichiometric mineral. Ricker and Osborn[24] reported that the olivine solid solution extends from the $CaMgSiO_4$ composition towards Mg_2SiO_4, but not towards merwinite. Strictly speaking, monticellite of the exact stoichiometric $CaMgSiO_4$ composition is not stable. Biggar and O'Hara[26] equilibrated this composition for 21 days at about 1500 °C and observed a mixture of 90% monticellite (olivine solid solution) and 10% merwinite identified by optical microscopy and X-ray diffraction. The instability of stoichiometric monticellite was also reported in other studies.[29–33]

The calculated Ca_2SiO_4–$CaMgSiO_4$ phase diagram section is compared with experimental data in Fig. 6. Because the existence of the "*T*" phase as a stable compound is still questionable, this phase is not shown. As seen on Fig. 6, Schlaudt and Roy[20] observed two or three phases in regions where the calculations indicate the existence of one or two phases, respectively. The phases were not identified by Schlaudt and Roy.[20] The most likely explanation is that the overall compositions of their samples did not lie exactly on the orthosilicate section.

Kosa et al.[34] reported the enthalpy of incongruent decomposition of merwinite into liquid, Ca_2SiO_4 and MgO at 1575 °C to be 125 ± 15 kJ/mol of merwinite. The calculated value is 120.0 kJ/mol at 1576 °C.

Fig. 7 compares the calculated $CaMgSiO_4$–Mg_2SiO_4 phase diagram section with experimental data. The solubility of monticellite in forsterite and vice versa (that is, the miscibility gap in the olivine solution) and the non-stoichiometry of monticellite are well reproduced. Fig. 8 shows an enlargement of the peritectic melting of monticellite (olivine solid solution). In the previous assessment by Huang et al.,[6] the range of stoichiometry of monticellite (olivine) was shown extending from the $CaMgSiO_4$ composition not only towards the Mg_2SiO_4 side, but also towards the Ca_2SiO_4 side in contradiction to several studies mentioned above.[26,29–33] The liquidus of MgO at the monticellite composition measured by Ricker and Osborn[24] is substantially lower than the calculated liquidus which is consistent with the results of Osborn[23] and Ricker and Osborn at other compositions. This could result from a small deviation of their experimental samples from the orthosilicate section combined with the very steep MgO liquidus in that region (see Fig. 4). Overall, the calculated Ca_2SiO_4–Mg_2SiO_4 phase diagram section and the experimental data agree within experimental error limits.

Lumpkin and Ribbe[13] and Lumpkin et al.[14] studied the distribution of Ca^{2+} and Mg^{2+} cations between the M1 and M2 sites of the olivine solid solution by measuring lattice parameters. Ca^{2+}, with an ionic radius of 1.00 Å[35], strongly prefers the larger M2 sites, whereas Mg^{2+} (ionic radius of 0.72 Å[35]) is distributed between the M1 and M2 sites. The degree of disordering was determined from the *a* and *b* lattice parameters of olivine, which are affected sufficiently by the distribution of Ca and Mg cations. Adams and Bishop[27] used the same technique as Lumpkin et al. to study the cation distribution in olivine solutions from 1200 to 1400 °C. They found the amount of Ca on the M1 sites to be from 11 to 15% and 2 to 5% of the total Ca on the forsterite-rich side and monticellite-rich side of the miscibility gap, respectively. The calculated cation distribution in olivine is compared with experimental data in Fig. 9. The more ordered structure is calculated in monticellite at lower temperatures. This is consistent with the experimental data.

The olivine solution is modeled by the two-sublattice compound energy formalism. The Gibbs energies of three out of four end-members are known:[18,35] $(Mg)^{M2}(Mg)^{M1}SiO_4$ (forsterite), $(Ca)^{M2}(Ca)^{M1}SiO_4$ (γ-Ca_2SiO_4) and

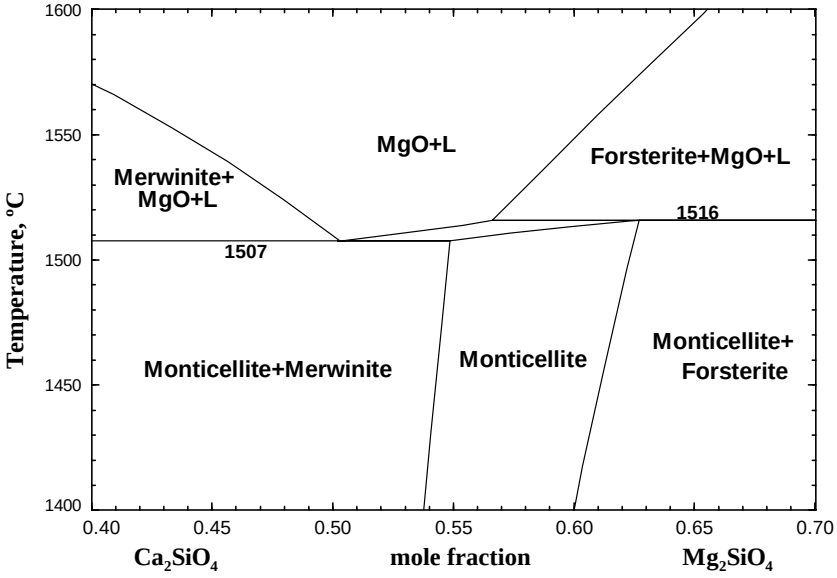

Fig. 8. Melting behavior of monticellite (olivine solid solution). Phase diagram is calculated from the optimization.

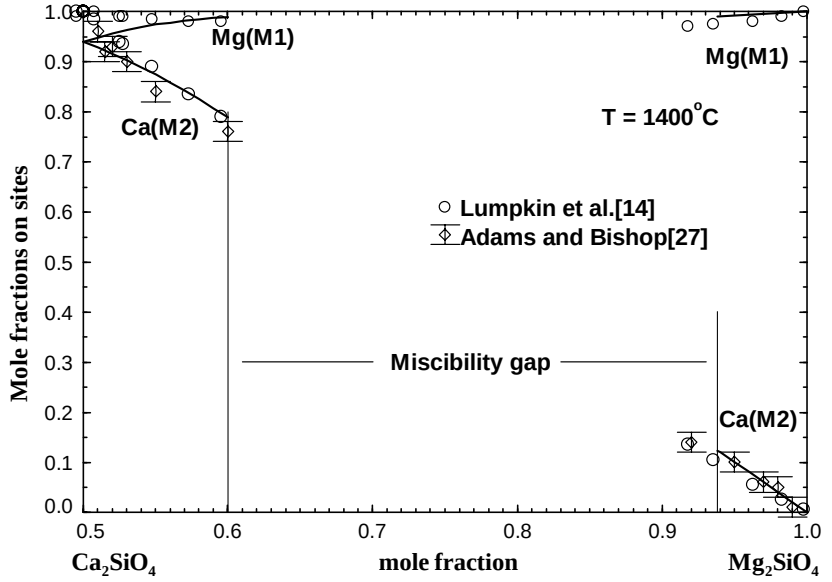

Fig. 9. Calculated cation distribution of Ca and Mg between M2 and M1 sites in olivine solid solutions at 1400 °C. Mole fractions of Ca and Mg on M2 and M1 sites.

$(Ca)^{M2}(Mg)^{M1}SiO_4$ (monticellite). The Gibbs energy of $(Mg)^{M2}(Ca)^{M1}SiO_4$ was optimized as shown in Table 2 to reproduce the measured cation distribution. In order to reproduce the measured phase-equilibrium diagrams, two miscibility gaps are necessary, on the Mg_2SiO_4–$CaMgSiO_4$ side and on the Ca_2SiO_4–$CaMgSiO_4$ side. The miscibility gap between monticellite and forsterite was modeled using an asymmetric $L_{Ca,Mg:Mg}$ ($=L_{Ca,Mg:Ca}$) parameter. The second miscibility gap between γ-Ca_2SiO_4 and monticellite was modeled using the parameter $L_{Ca:Ca,Mg}$ ($=L_{Mg:Ca,Mg}$). Without this gap, merwinite becomes thermodynamically unstable. The model parameters are listed in Table 2.

3.2. Metasilicate section

Fig. 10 shows the calculated phase diagram of the $CaSiO_3$–$MgSiO_3$ metasilicate section. The phase equilibria between the pyroxene solutions are very complicated in the $CaMgSi_2O_6$ (diopside)–$Mg_2Si_2O_6$ (enstatite) region. Wollastonite dissolves up to about 10 mol% of $MgSiO_3$, while pseudo-wollastonite is a stoichiometric compound.

The phase equilibria in the diopside–enstatite section, which are of particular importance in geochemistry, have been studied extensively. Bowen[36] investigated the phase equilibria in the forsterite–diopside–SiO_2 section using the

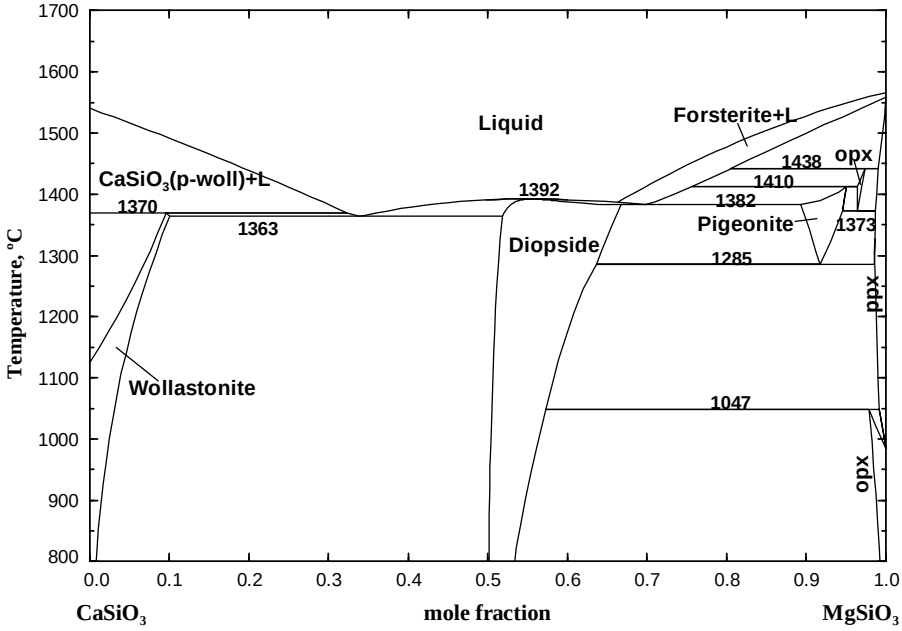

Fig. 10. Calculated phase diagram of the $CaSiO_3$–$MgSiO_3$ metasilicate section.

quenching technique followed by optical microscopic phase determination. In the experiments, primary crystallization of SiO_2, pyroxene and forsterite was detected. Moreover, the phase diagrams of the diopside–enstatite, diopside–SiO_2 and diopside–forsterite pseudo-binary joins were measured. Boyd and Schairer[37] studied the diopside–enstatite section using the quenching technique followed by optical microscopic and X-ray phase determination. The liquidus was measured for forsterite and pyroxene solutions. The phase equilibria between diopside and enstatite (proto- and ortho-pyroxene) solid solutions were studied in the temperature range between 800 and 1380 °C. The compositions of the solid solutions were determined by X-ray measurements of lattice parameters. Kushiro[38] studied the forsterite–diopside–silica system using electron probe analysis of quenched samples. The phase equilibria between enstatite and diopside were measured and a small deviation of the diopside solid solution from the metasilicate section towards lower silica was reported. Schairer and Yoder[39] studied phase equilibria in the forsterite–diopside–silica system below 1410 °C using the quenching technique. Kushiro and Schairer[40] obtained the diopside–enstatite phase diagram using the quenching technique and reported a maximum on the diopside liquidus at about 90% $CaMgSi_2O_6$. Yang[41] and Longhi[42] studied the metastable phase equilibria of ortho-pyroxene in the metasilicate section.

The phase diagram of the diopside–enstatite section was constructed by Longhi and Boudreau[43] based on measurements of the ortho-enstatite liquidus in the forsterite–diopside–SiO_2 system using the quenching technique followed by EPMA (EDS) and X-ray phase analysis. Jenner and Green[44] determined the phase equilibria in the Mg-rich part of the pyroxene quadrilateral $Mg_2Si_2O_6$–$CaMgSi_2O_6$–$CaFeSi_2O_6$–$Fe_2Si_2O_6$. Biggar[45] reviewed the compositions of proto-pyroxene, ortho-pyroxene and pigeonite (clino-pyroxene), coexisting with liquid in the CaO–MgO–SiO_2 system using previously published data and his new data obtained by X-ray diffraction on quenched samples. Recently, a more accurate phase diagram was proposed by Carlson[46] based on his own experiments as well as on previous studies. Carlson measured the phase equilibria between pyroxene solid solutions in the enstatite–diopside section over the temperature range from 925 to 1425 °C. Each point on a phase boundary was bracketed by two measured compositions. V_2O_5 and PbO solvents were used to facilitate equilibration and to promote crystal growth to sizes permitting unambiguous phase identification by X-ray diffraction and accurate chemical analysis by the electron microprobe, thereby resolving substantial discrepancies among previous studies of pyroxene phase equilibria.

Fig. 11 compares the calculated phase diagram of the $CaMgSi_2O_6$–$Mg_2Si_2O_6$ section with experimental data. Diopside and forsterite (olivine containing less than 1 mol% of Ca_2SiO_4) appear as primary crystalline phases. Pigeonite and diopside have the same clino-pyroxene structure. Ortho-pyroxene reappears in the narrow temperature range between 1373 and 1441 °C. The calculated liquidus of forsterite is systemically lower than the experimental data of Bowen[36] by about 30 °C. This could be the result of a small deviation of the experimental samples from the metasilicate stoichiometry combined with the steep slope of the forsterite liquidus. (A section calculated at $X_{SiO_2} = 0.49$ is in good agreement with the experimental liquidus.) An enlargement of the small pigeonite and ortho-pyroxene fields is shown in Fig. 12.

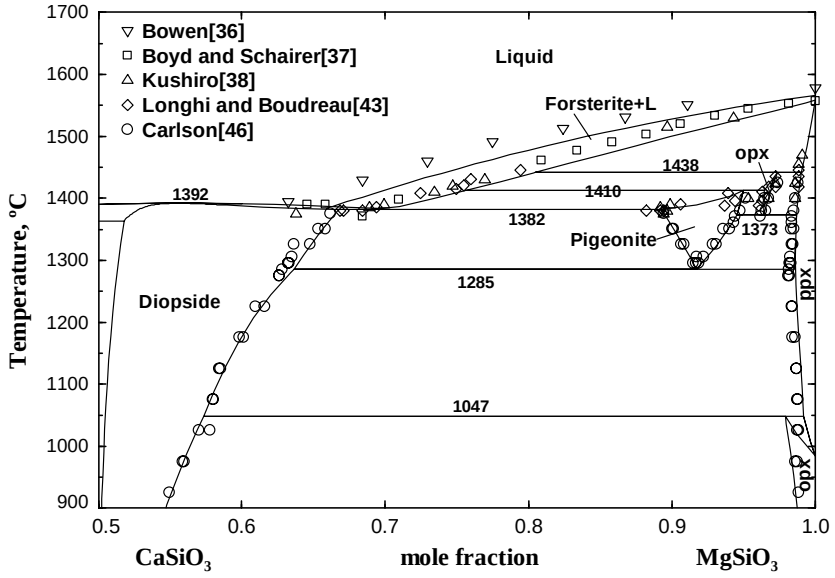

Fig. 11. Calculated phase diagram of the $CaMgSi_2O_6$–$MgSiO_3$ section.

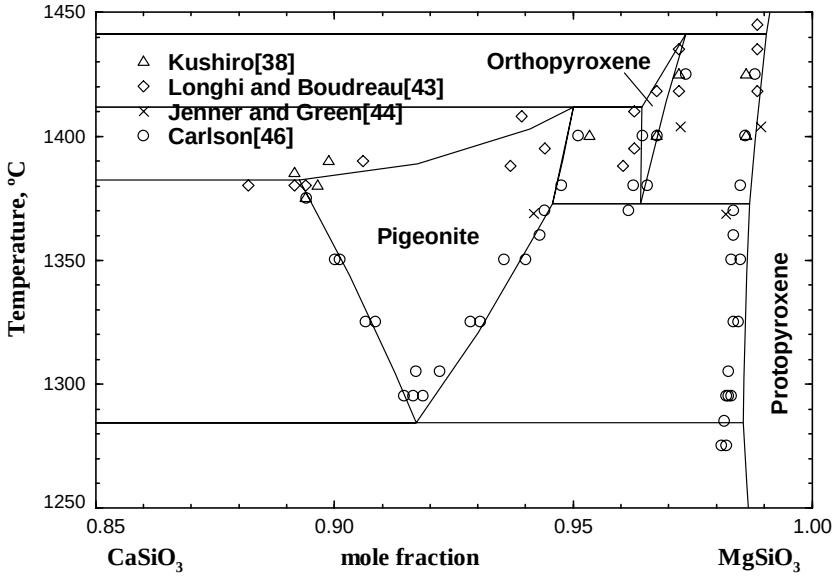

Fig. 12. Enlargement of the calculated phase diagram around the pigeonite (clino-pyroxene) region in the metasilicate section.

Fig. 13 shows the calculated enthalpy of the $CaMgSi_2O_6$–$Mg_2Si_2O_6$ clino-pyroxene solution at 970 K. Newton et al.[47] measured the enthalpy of dissolution of synthetic clino-pyroxenes in $2PbO{\cdot}B_2O_3$ melts at 970 K. The measured enthalpy showed positive deviations from ideality. This is well reproduced by the calculated curve in Fig. 13. This positive deviation implies the existence of a miscibility gap in the clino-pyroxene solution.

Before modeling the pyroxene solutions, the Gibbs energies of the $MgSiO_3$ enstatite phases had to be determined because the phase transformations of enstatite were not well treated in the previous optimization of the MgO–SiO_2 binary system.[11] The Gibbs energies of different crystal modifications of enstatite, $MgSiO_3$, were taken from the assessment of Huang et al.[6] and then slightly modified to reproduce the metastable phase transitions of enstatite. Perrotta and Stephenson[48] and Smith[49] reported the metastable transformation from low clino-enstatite to clino-enstatite at about 995 °C. The transition temperature calculated in the present study is 978 °C. Newton et al.[47] estimated the enthalpy of transition from clino-enstatite to ortho-enstatite to be about -4.6 ± 0.45 kJ/mol at 970 K from extrapolation of the measured enthalpy of dissolution of the clino-pyroxene solution to the pure $MgSiO_3$ composition and from the dissolution enthalpy of ortho-enstatite. If the enthalpy of dissolution of ortho-enstatite obtained by Shearer and Kleppa[50] is used instead of the value of Newton et al., the corresponding enthalpy of transition is -3.6 ± 0.6 kJ/mol. In the present

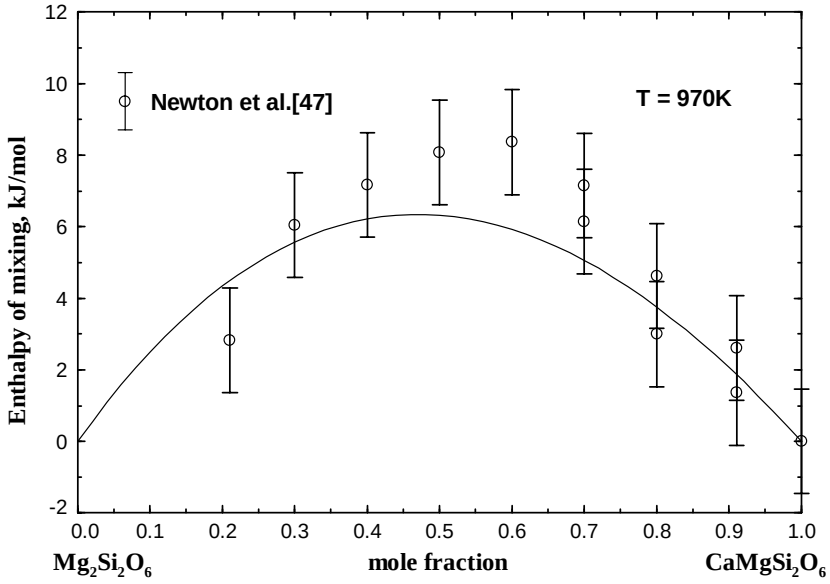

Fig. 13. Calculated enthalpy of mixing of the clino-pyroxene solution at 970 K.

study, the enthalpy of transition from clino-enstatite to ortho-enstatite is calculated to be −3.55 kJ/mol. The slightly modified Gibbs energies of Huang et al.[6] are now stored in the F*A*C*T database.[35] It should be noted that the Gibbs energies of ortho- and proto-enstatite used in the present study are very close to Berman's recommended values.[18]

The pyroxene solutions were modeled based on the calorimetric data (Fig. 13) and the phase diagram (Fig. 11). Clino-pyroxene was modeled first, taking advantage of the available thermodynamic data. Pigeonite and diopside have the same clino-pyroxene structure and are modeled as one solution with a miscibility gap. A slightly asymmetric interaction energy involving ${}^{0}L_{\mathrm{Ca,Mg:Mg}}$ and ${}^{1}L_{\mathrm{Ca,Mg:Mg}}$ parameters was found necessary to reproduce the measured miscibility gap between diopside and pigeonite. Low clino-pyroxene and proto-pyroxene were modeled using similar excess parameters and optimized Gibbs energies of the $CaMgSi_2O_6$ end-members as shown in Table 2. The excess parameters for all pyroxene phases can be seen in Table 2 to have very similar numerical values except in the case of ortho-pyroxene. An interaction energy $L_{\mathrm{Ca,Mg:Mg}}$ with negative temperature dependence was necessary to reproduce the reappearance of ortho-pyroxene at high temperatures.

The calculated phase diagram of the $CaSiO_3$–$CaMgSi_2O_6$ section is compared with experimental data in Fig. 14. Allen et al.[51] were the first to study the phase relations

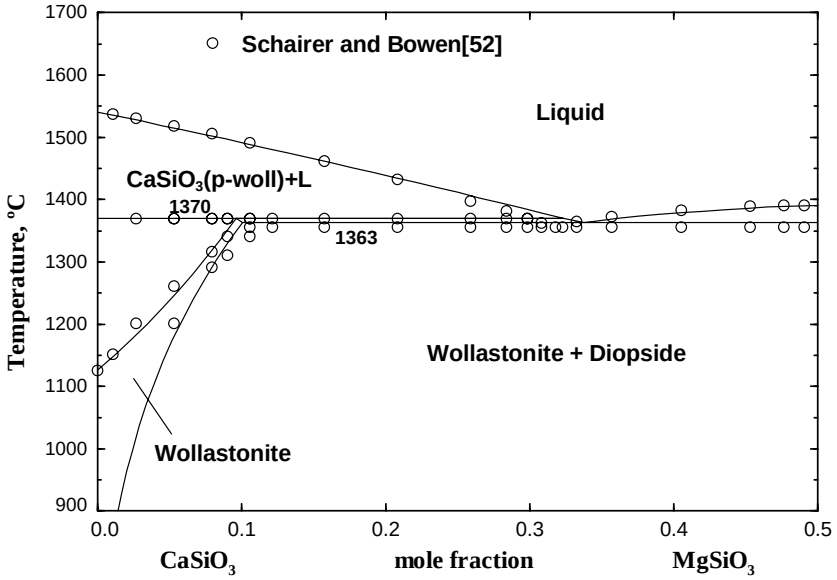

Fig. 14. Calculated phase diagram of the $CaSiO_3$–$CaMgSi_2O_6$ section.

in this section. They used heating curves and microscopic phase examination. They reported the presence of up to 17 wt.% of diopside in wollastonite, about 3–4 wt.% of diopside in pseudo-wollastonite and less than 3 wt.% of $CaSiO_3$ in diopside. Ferguson and Merwin[31] investigated the CaO–MgO–SiO_2 system below 1600 °C using a quenching technique followed by microscopic phase determination. The solid solution of diopside in wollastonite was observed. Later, Schairer and Bowen[52] used the same method for a thorough study of phase equilibria between $CaSiO_3$ and diopside. They concluded that a maximum of 22 wt.% diopside dissolves in wollastonite and there is almost no solubility of wollastonite in diopside. Osborn[53] measured the primary crystallization region of the wollastonite solution in the CaO–MgO–SiO_2 system using quenching in combination with optical microscopic phase determination. The calculated diagram is in good agreement with the experimental data of Schairer and Bowen. No excess Gibbs energy parameter was necessary to model wollastonite. However, the Gibbs energy of the fictive $MgSiO_3$ end-member was optimized as shown in Table 2.

Tarina et al.[54] used transposed-temperature drop calorimetry to measure the enthalpy change for the heating and melting of (pseudo-wollastonite + diopside) mixtures (see Fig. 15). The results showed a very small negative enthalpy of mixing. DeYoreo et al.[55] measured the heat content of the mixture of wollastonite and diopside (83 mol% diopside) using a scanning calorimetric technique in the temperature range from 1375 to 1750 K. Navrotsky et al.[56] and Ziegler and Navrotsky[56,57] obtained the heat content of diopside using drop calorimetry. The incongruent melting behavior of diopside above 1634 K was observed. Lange et al.[58] measured the heat content of diopside between 1403 and 1763 K using scanning calorimetry. They found that incongruent melting begins approximately at 1606 K. Stebbins et al.[59] and Richet and Bottinga[60] also reported the heat content of the liquid at the diopside composition. Their data are in agreement with the measurements of Lange et al.[58]

The enthalpy of the liquid phase between the $CaSiO_3$ and diopside compositions, and the enthalpy of melting of diopside are calculated in Figs. 15 and 16. The calculated curves are in excellent agreement with experimental data. In particular, in the case of the enthalpy change during the melting of stoichiometric diopside, the incongruent melting behavior pointed out by Ziegler and Navrotsky[56,57] is well reproduced. This can be understood by reference to Fig. 16. Diopside begins to melt at 1636 K and melting is complete at 1665 K. The calculated enthalpy of fusion is 129.6 kJ/mol, which is slightly lower than the experimental data.[54,55,57–61] The measurements of DeYoreo et al.[55] are also well reproduced by the calculations.

3.3. Other phase diagram sections

The calculated phase diagram of the diopside–forsterite section is compared with the experimental data in Fig. 17. Bowen[36] measured the liquidus of forsterite in this section using a quenching technique and optical microscopic phase determination, and suggested that this system is a quasi-binary system with a eutectic at 12 wt.% forsterite and 1387 °C. Later, the phase equilibria in the diopside–forsterite section were studied by Kushiro and Schairer[40] using a quenching technique followed by X-ray diffraction. The diopside and forsterite solutions were found to be in equilibrium with compositions off this join. Therefore, the diopside–forsterite section is not a true quasi-binary system. It was reported that forsterite can contain up to about

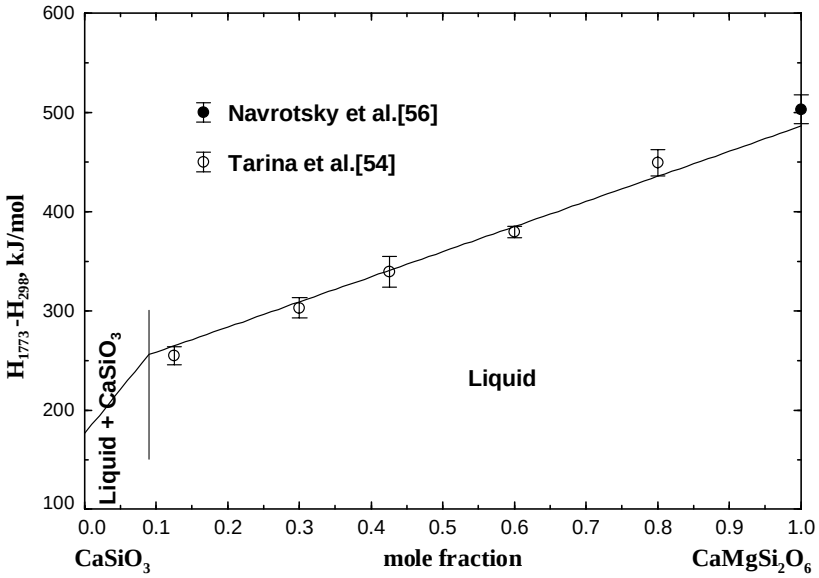

Fig. 15. The calculated and experimental enthalpy change for the heating and melting of (pseudowollastonite + diopside) mixtures.

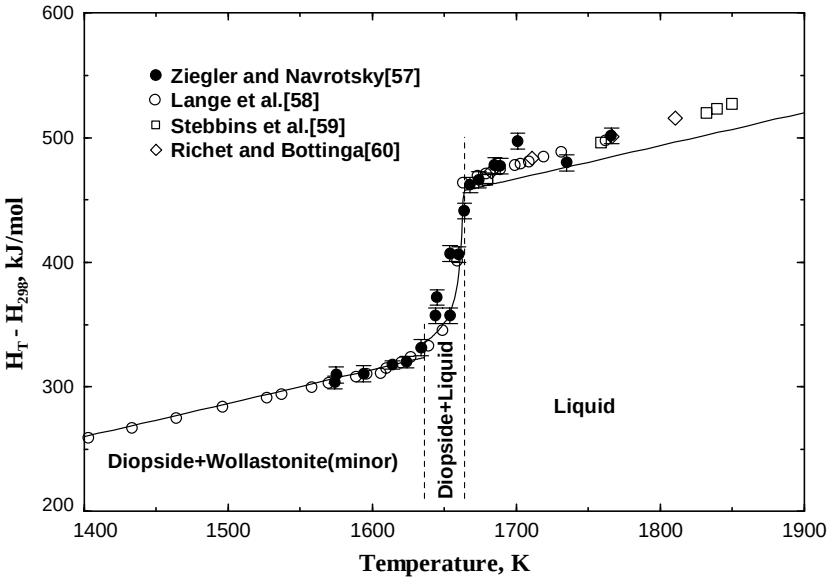

Fig. 16. Comparison of calculated and experimental enthalpy at the stoichiometric $CaMgSi_2O_6$ composition.

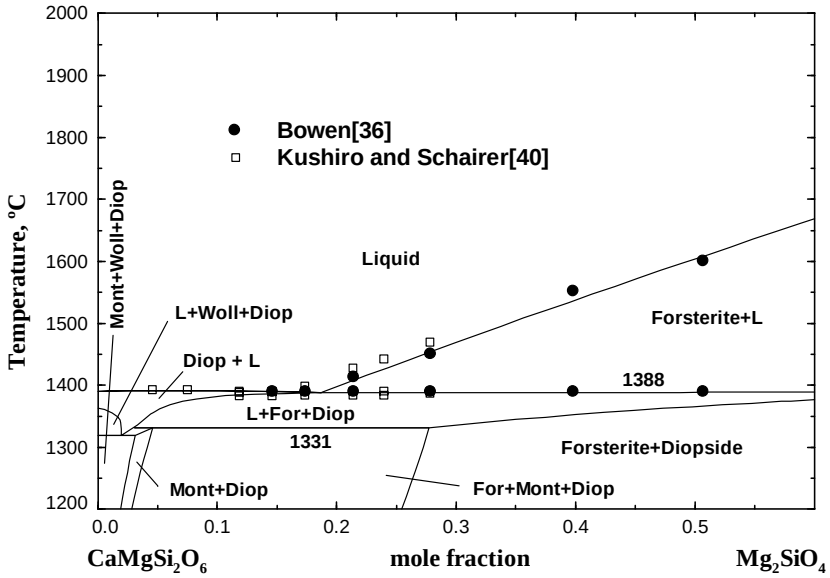

Fig. 17. Calculated phase diagram of the $CaMgSi_2O_6$–Mg_2SiO_4 section.

8 mol% of monticellite in equilibrium with the diopside solution at 1350 °C. The value calculated in the present study from the optimized model parameters is 11 mol%. As can be seen from Fig. 17, the calculated liquidus and the phase boundary of diopside are in good agreement with the experimental data. The eutectic point mentioned by Bowen is actually a saddle point (see also Fig. 4).

The calculated phase diagram of the diopside–SiO_2 section is shown in Fig. 18. This section was also first studied by Bowen.[36] Schairer and Kushiro[62] found a three-phase region (diopside + SiO_2 + liquid) and reported that X-ray patterns of diopside coexisting with liquid or with liquid and tridymite were different from those of pure diopside. They concluded that the diopside–SiO_2 section is not a true quasi-binary system. Diopside was reported to dissolve up to 7.5 mol% of enstatite based on X-ray diffraction analysis. The calculated maximum solubility is about 8.5 mol% $Mg_2Si_2O_6$. The calculated phase diagram is in excellent agreement with the experimental data.

The phase diagrams of the diopside-akermanite and $CaSiO_3$–akermanite sections are given in Figs. 19 and 20. Kushiro and Schairer[63] obtained the phase diagram of the diopside-akermanite section using a quenching technique followed by X-ray analysis. They reported up to about 5 mol% solubility of akermanite in diopside at 1355 °C based on X-ray measurements of the diopside lattice parameters. A very small solubility of akermanite in diopside was also deduced by Valley and Essene[64] from the simi-

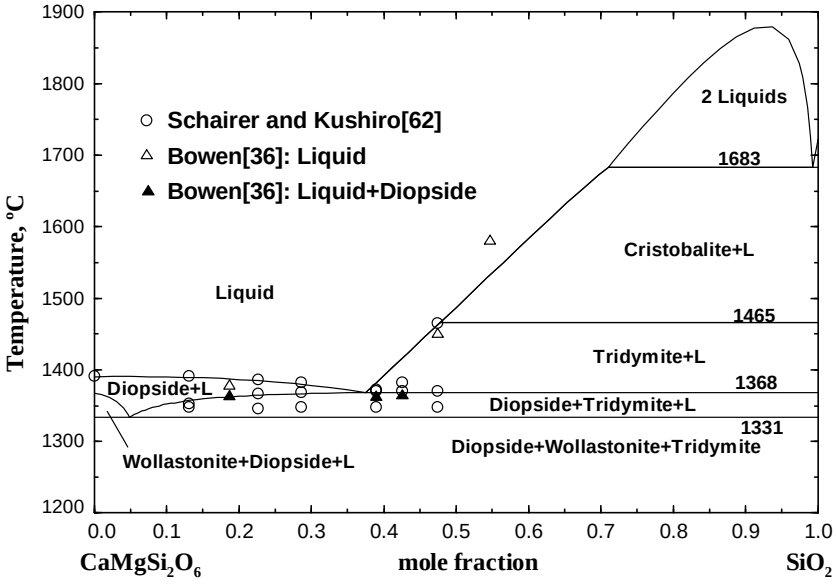

Fig. 18. Calculated phase diagram of the $CaMgSi_2O_6$–SiO_2 section.

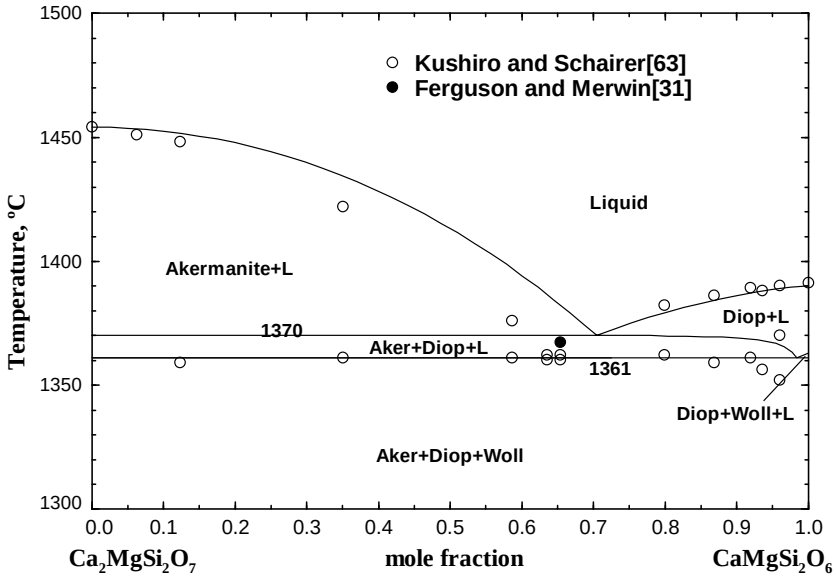

Fig. 19. Calculated phase diagram of the $Ca_2MgSi_2O_7$–$CaMgSi_2O_6$ section.

lar X-ray experiments on the quenched samples from the earlier study[22] which contained both diopside and akermanite. A substantial solubility of akermanite in diopside seems unlikely and was neglected in the present study. More direct evidence such as EPMA measurements, is needed to prove the extension of the diopside solid solution towards akermanite. The minimum on the liquidus in the $Ca_2MgSi_2O_7$–$CaMgSi_2O_6$ section was measured at 1367 °C in the quenching experiments of Ferguson and Merwin.[31]

Schairer and Bowen[65] studied the phase equilibria in the $CaSiO_3$–akermanite section using a quenching technique and microscopic phase determination. They found no solid solutions in this section contrary to the earlier study of Ferguson and Merwin[31] who reported that the wollastonite solid solution extended towards akermanite.

Yoder[66,67] suggested that akermanite may form a solid solution with other phases in the CaO–MgO–SiO_2 system at about 10 kbar. The EPMA study of Yoder's samples[66] at about 5–10 kbar by Sharp et al.[21] revealed the possibility of up to 2% substitution of Mg for Ca in $Ca_2MgSi_2O_7$. On the other hand, a constant (Ca + Mg)/Si ratio of 3/2 was obtained, indicating no detectable solid solution towards olivine. In the present study, akermanite is assumed to be a stoichiometric compound at ambient pressure.

Proks et al.[68] measured the heat content of akermanite from 1469 to 1865 K using drop calorimetry. The enthalpy of fusion of akermanite at its melting tempera-

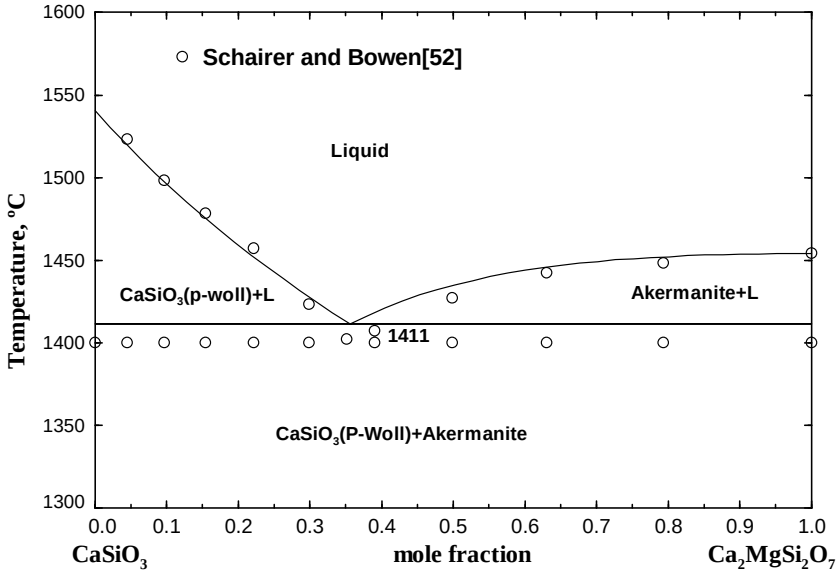

Fig. 20. Calculated phase diagram of the $CaSiO_3$–$Ca_2MgSi_2O_7$ section.

ture of 1725 K was found to be 123.9 ± 3.2 kJ/mol. The calculated enthalpy of fusion is 118.7 kJ/mol at 1727 K. Adamkovicova et al.[69,70] measured the enthalpy of melts in the $CaSiO_3$–akermanite section over the temperature range from 1760 to 1930 K using high-temperature drop calorimetry and solution calorimetry. The enthalpy of mixing was found to be almost zero at any composition. The calculated enthalpy of mixing of the akermanite–$CaSiO_3$ liquid shows a minimum of −1.4 kJ/mol at a mole fraction of $CaSiO_3$ equal to 0.62 which is in agreement with the calorimetric data within experimental error limits.

The calculated phase diagrams of the Ca_2SiO_4–akermanite, merwinite–akermanite and monticellite–akermanite sections are presented in Figs. 21–23. Osborn[23] investigated the first two sections by quenching experiments and microscopic phase determination. The Ca_2SiO_4 and merwinite phases were not distinguishable by microscopic analysis. Osborn[23] reported problems with quenching for most of the studied compositions. Instead of the glass phase, a product of devitrification was commonly observed in quenched samples. The calculated liquidus is somewhat lower than the experimental data.[23] This is most likely due to the unquenchability of the liquid.

Osborn[23] tried to establish the primary phase region of rankinite, $Ca_3Si_2O_7$. The exaggerated rankinite primary region in his tentative phase diagram is not supported by solid experimental evidence. The rankinite primary phase region calculated in the present study is very small as can be seen

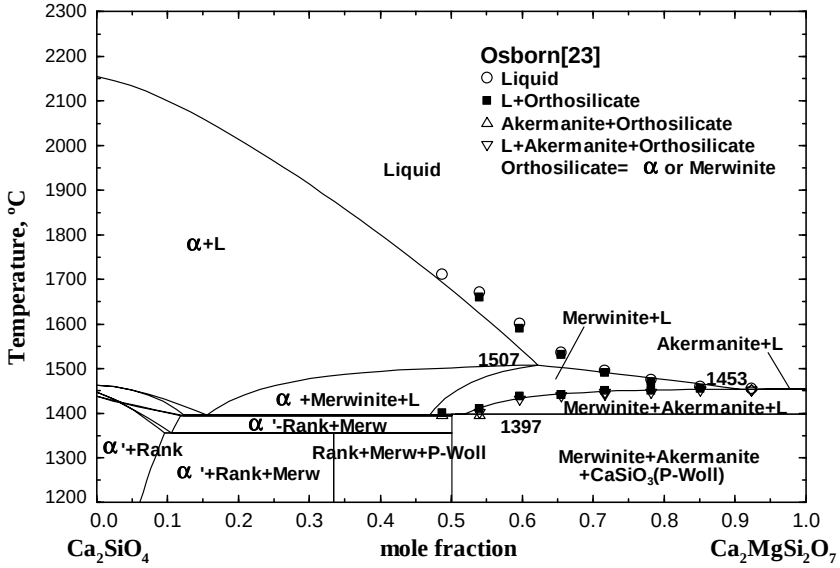

Fig. 21. Calculated phase diagram of the Ca_2SiO_4–$Ca_2MgSi_2O_7$ section.

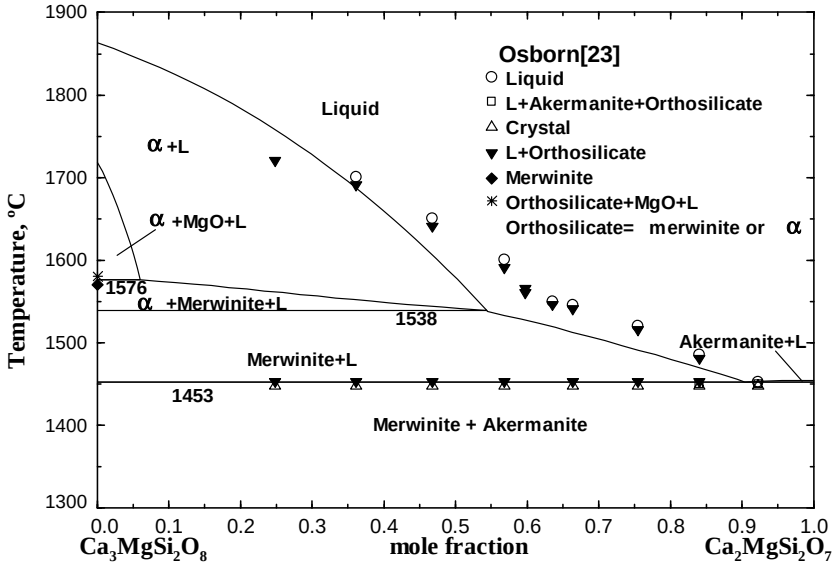

Fig. 22. Calculated phase diagram of the $Ca_3MgSi_2O_8$–$Ca_2MgSi_2O_7$ section.

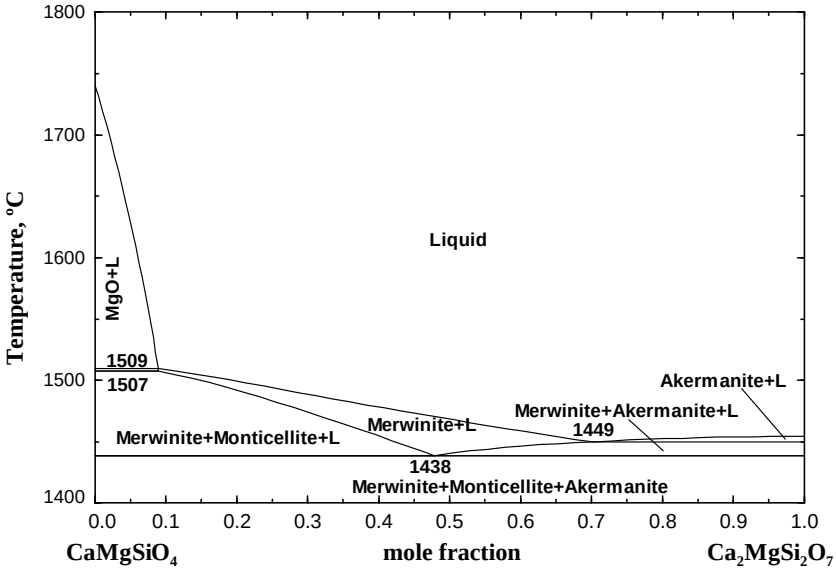

Fig. 23. Calculated phase diagram of the $CaMgSiO_4$–$Ca_2MgSi_2O_7$ section.

from Fig. 4. Similarly, the primary crystallization field of Ca_3SiO_5 was exaggerated in the tentative phase diagram of Ricker and Osborn.[24] Since quenching of liquid is problematic in this area, a substantial primary phase region of Ca_3SiO_5 is not supported by direct experimental evidence. Even in the binary CaO–SiO_2 system, several experimental studies reported contradictory results on the upper temperature of stability of Ca_3SiO_5. In the latest optimization of the CaO–SiO_2 system (see Fig. 2), preference was given to the experimental data indicating decomposition of Ca_3SiO_5 below the liquidus. Therefore, there is no primary field of this compound on the calculated liquidus projection shown in Fig. 4.

Spencer et al.[71] measured several tie-lines between liquid and forsterite or periclase at 1800 °C using an air quenching technique followed by X-ray diffraction and EPMA analysis. Sakai and Suito[72] measured the liquidus of forsterite, periclase and Ca_2SiO_4 at 1600 °C using equilibration in MgO or Pt crucibles followed by quenching and EPMA or inductively couple plasma analysis. These phase-equilibrium data are also well reproduced by the calculations based on the optimized model parameters (see the corresponding isotherms in Fig. 4).

Greig[73] studied the (two liquids + crystobalite) univariant line by a quenching technique and microscopic analysis. He found this line to be slightly convex, whereas a slightly

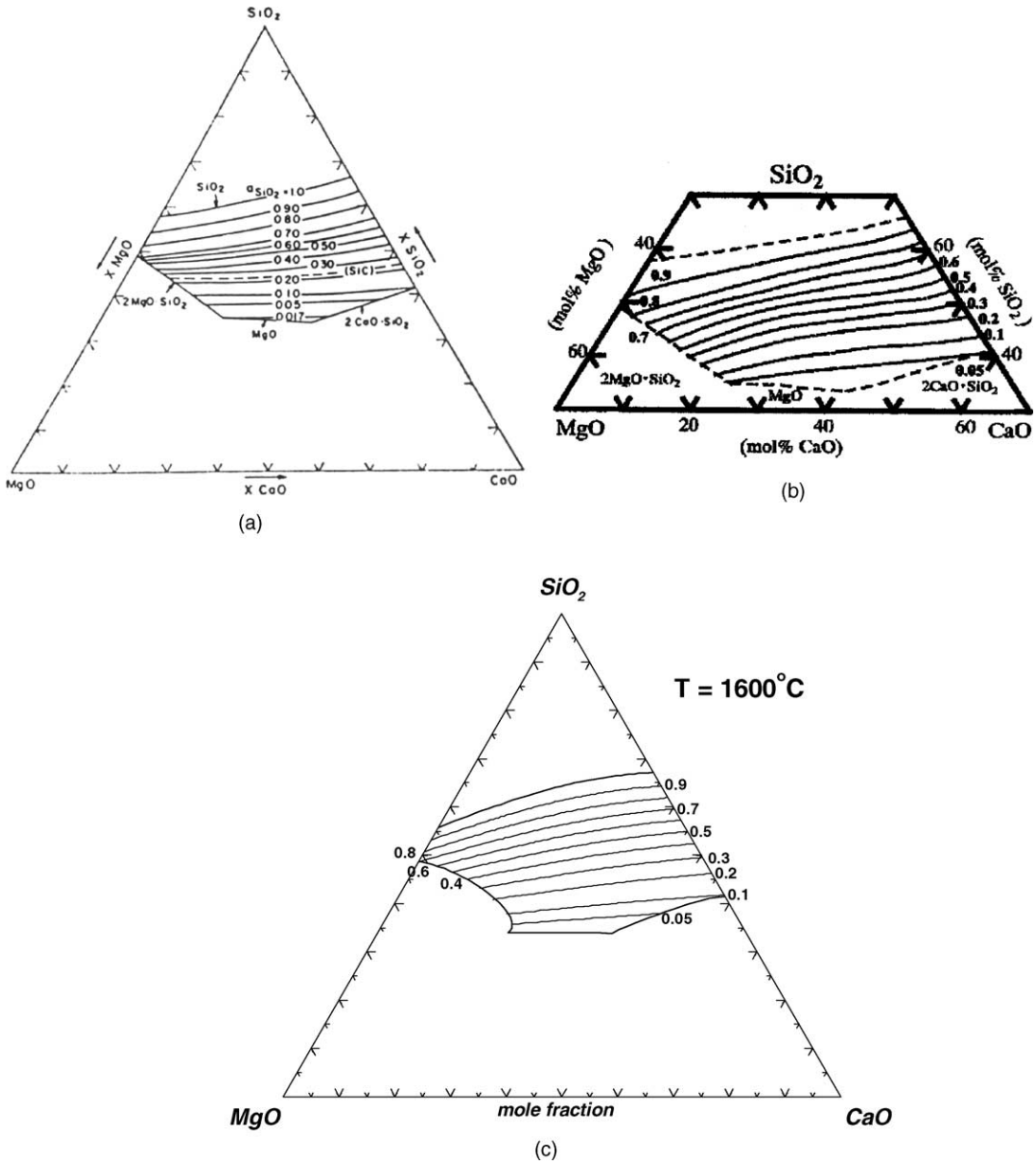

Fig. 24. Activities of SiO_2 (relative to solid cristobalite) in the CaO–MgO–SiO_2 liquid slag at 1600 °C: (a) Rein and Chipman,[77] (b) Morita et al.,[78] (c) calculated in the present study.

concave univariant line is calculated in the present study (see Fig. 4). It should be noted that the latter shape is due to the contribution of the configurational entropy to the Gibbs energy of liquid and this shape is found in many similar ternary systems. The liquid miscibility gap was also studied by Kirschen and DeCapitani[74] at temperatures up to 1940 °C using the levitation technique. A few tie-lines were obtained by EPMA analysis of quenched samples.

3.4. Sub-solidus equilibria

Harker and Tuttle[75] and Yoder[22] determined the low-temperature stability limit of akermanite. The temperature versus pressure univariant line was obtained for the equilibrium reaction (wollastonite + monticellite = akermanite) from 6 to 0.8 kbar total pressure. Extrapolation of these data to ambient pressure suggests that akermanite dissociates into wollastonite and monticellite below about 700 °C. The dissociation temperature calculated in the present study is 701 °C.

Walter[76] and Yoder[22] obtained the pressure versus temperature univariant line for the equilibrium (diopside + monticellite = forsterite + akermanite) from 5 to 1 bar. They found that the equilibrium low temperature phase assemblage (diopside + monticellite) gave way to the (forsterite + akermanite) assemblage above about 870 °C at ambient pressure. The calculated transition temperature is 838 °C.

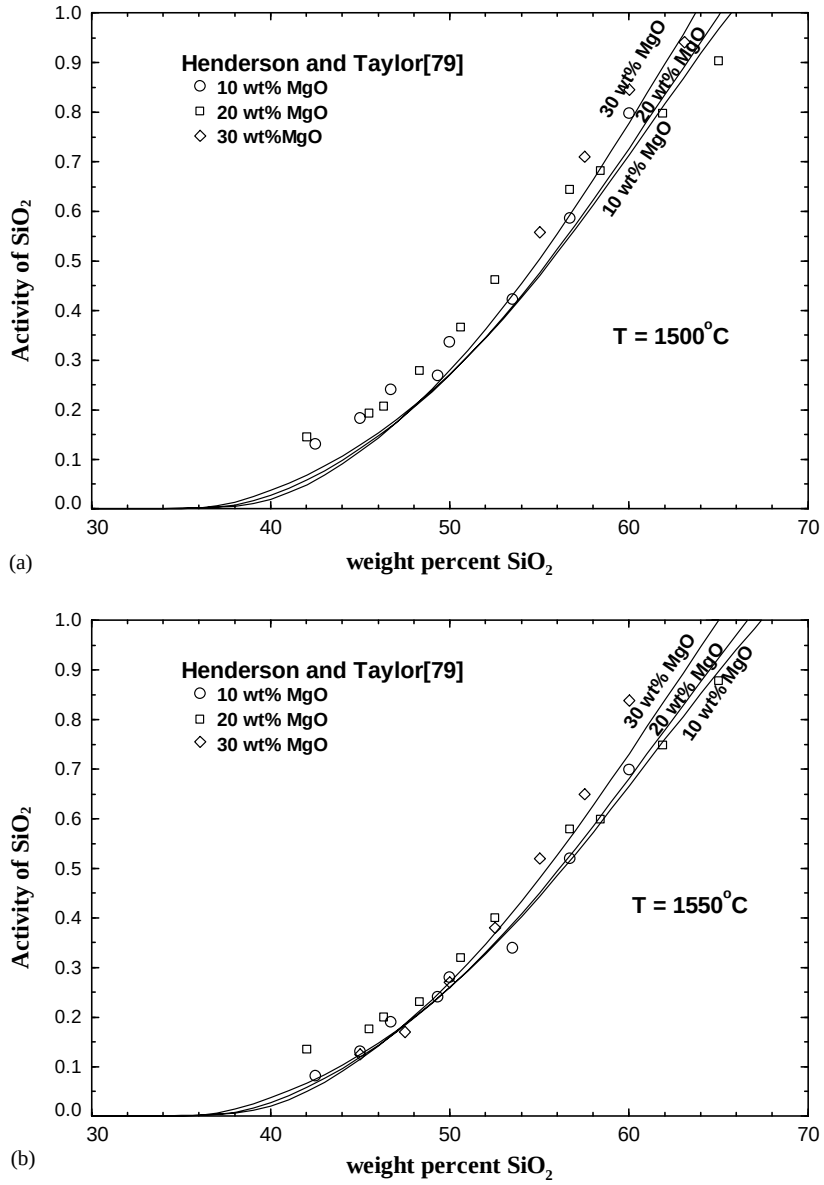

Fig. 25. Comparison of the calculated activities of SiO_2 (relative to solid cristobalite standard state) in the CaO–MgO–SiO_2 slag with experimental data by Henderson and Taylor:[79] (a) 1500 °C and (b) 1550 °C.

3.5. Activities of components in molten oxide

Rein and Chipman[77] obtained the activities of silica in the CaO–MgO–SiO_2 liquid at 1600 °C from the compositions of the slag and Fe–Si–C alloys equilibrated in carbon or silicon carbide crucibles in atmospheres of CO. Morita et al.[78] also reported the activities of SiO_2 in the slag at 1600 °C based on equilibration of the slag and Si alloys in graphite crucibles. The measured compositions of the slag and alloy in combination with known Henrian activity coefficients of Ca and Mg in Si alloys allowed the authors to calculate the activities of all slag components using the Gibbs–Duhem relationship. The results of Morita et al.[78] and Rein and Chipman[77] are compared with the activities of SiO_2 calculated in the present study in Fig. 24.

Henderson and Taylor[79] determined the activity of silica in CaO–MgO–SiO_2 liquid slags saturated with both graphite and SiC at 1500 and 1550 °C by measuring the slag composition and the equilibrium pressure of CO. Fig. 25 shows these experimental data and the calculated activities of SiO_2 in slags of constant MgO content. The activities of CaO in the CaO–MgO–SiO_2 slag were reported in two studies.[80,81] The first set of data was obtained by a complex emf technique at 1600 °C. In the second study, the CaO activities in the slag at 1500 °C were calculated from the equilibrium constant of the reaction ($CaO + 1/2S_2 = CaS + 1/2O_2$) The composition of the slag was measured, including the CaS content. The activity coefficient of CaS in the slag was assumed to be equal to 1.0, and the partial pressures of O_2 and S_2 were calculated from the equilibrium gas composi-

tion. The reliability of the reported[80,81] CaO activities is believed to be relatively low due to experimental difficulties, the assumptions made in calculating the activities, and the sensitivity of small activity values to experimental errors.

4. Conclusions

A complete critical evaluation of all available phase diagram, thermodynamic and structural data for the CaO–MgO–SiO_2 system at a total pressure of 1 bar has been made, and parameters of thermodynamic models have been optimized to reproduce all experimental data within experimental error limits. The evaluation/optimization of the CaO–MgO–SiO_2 system reported in this study is part of a wider research program aimed at complete characterization of phase equilibria and thermodynamic properties of the entire six-component system CaO–MgO–Al_2O_3–FeO–Fe_2O_3–SiO_2, which has numerous applications in the ceramic, cement and glass industries, metallurgy, geochemistry, etc. The model parameters obtained in this study are included in the general F*A*C*T[35] database of optimized model parameters for the CaO–MgO–Al_2O_3–FeO–Fe_2O_3–SiO_2 system. This database can be readily used with software for Gibbs energy minimization in order to calculate any phase equilibrium or phase diagram of interest.

Acknowledgements

This project was supported by a CRD grant from the Natural Sciences and Engineering Research Council of Canada in collaboration with INCO, Noranda, Rio Tinto, Teck Cominco, Alcoa, Dupont, Shell, Corning, Pechiney, Norsk Hydro, Sintef, Schott Glas, St.-Gobain Recherche, Mintek and IIS Materials.

References

1. Pelton, A. D. and Eriksson, G. A., Thermodynamic database computing system for multicomponent glasses. In *Advances in the Fusion of Glasses*. American Ceramic Society, Westerville, OH, 1988, pp. 27.1–27.11.
2. Pelton, A. D. and Blander, M., Computer-assisted analysis of the thermodynamic properties and phase diagrams of slags. In *Proceedings of the Second International Symposium on Metallurgical Slags and Fluxes*. TMS-AIME, Warrendale, PA, 1984, pp. 281–294.
3. Pelton, A. D. and Blander, M., Thermodynamic analysis of ordered liquid solutions by a modified quasi-chemical approach. application to silicate slags. *Metall. Trans. B* 1986, **17B**, 805–815.
4. Pelton, A. D., Decterov, S. A., Eriksson, G., Robelin, C. and Dessureault, Y., The modified quasichemical model. I—binary solutions. *Metall. Mater. Trans. B* 2000, **31B**, 651–659.
5. Pelton, A. D. and Chartrand, P., The modified quasichemical model. II—multicomponent solutions. *Metall. Mater. Trans. A* 2001, **32A**, 1355–1360.
6. Huang, W., Hillert, M. and Wang, X., Thermodynamic assessment of the CaO–MgO–SiO_2 system. *Metall. Mater. Trans. A* 1995, **26A**, 2293–2310.
7. Hillert, M., Jansson, B. and Sundman, B., Application of the compound-energy model to oxide systems. *Z. Metallkd.* 1988, **79**, 81–87.
8. Hillert, M., Jansson, B. and Sundman, B., A two-sublattice model for molten solutions with different tendency for ionization. *Metall. Trans. A* 1985, **16A**, 261–266.
9. Wu, P., Eriksson, G. and Pelton, A. D., Critical evaluation and optimization of the thermodynamic properties and phase diagrams of the calcia-iron(II) oxide, calcia-magnesia, calcia-manganese(II) oxide, iron(II) oxide-magnesia, iron(II) oxide-manganese(II) oxide, and magnesia-manganese(II) oxide systems. *J. Am. Ceram. Soc*. 1993, **76**, 2065–2075.
10. Eriksson, G., Wu, P., Blander, M. and Pelton, A. D., Critical evaluation and optimisation of the thermodynamic properties and phase diagrams of the MnO-SiO_2 and CaO–SiO_2 systems. *Can. Metall. Q*. 1994, **33**, 13–21.
11. Wu, P., Eriksson, G., Pelton, A. D. and Blander, M., Prediction of the thermodynamic properties and phase diagrams of silicate systems—evaluation of the FeO–MgO–SiO_2 System. *ISIJ Int.* 1993, **33**, 26–35.
12. Raeder, J. H., Holm, J. L. and Sorensen, O. T., Defects in metal-deficient cobalt-wustites (Co, Fe)$_{1-y}$O. *Solid State Ionics* 1984, **12**, 155–159.
13. Lumpkin, G. and Ribbe, P. H., Composition, order-disorder and lattice parameters of olivines: relationships in silicate, germanate, beryllate, phosphate, borate olivines. *Am. Miner.* 1983, **68**, 164–176.
14. Lumpkin, G. R., Ribbe, P. H. and Lumpkin, N. E., Composition, order-disorder and lattice parameters of olivines: determinative methods for Mg–Mn and Mg–Ca silicate olivines. *Am. Miner.* 1983, **68**, 1174–1182.
15. Deer, W. A., Howie, R. A. and Zussman, J., *An Introduction to the Rock Forming Minerals*. Longman House, Hong Kong, 1966.
16. Shi, P., Saxena, S. K., Zang, Z. and Sundman, B., Thermodynamics of the Ca–Mg–Fe–Al–Si–O pyroxenes: 1. Theoretical model and assessment of the Ca–Mg–Si–O system. *Calphad* 1994, **18**, 47–69.
17. Morimoto, N., Nomenclature of pyroxenes. *Miner. Mag.* 1988, **52**, 535–550.
18. Berman, R. G., Internally-consistent thermodynamic data for minerals in the system sodium oxide-potassium oxide-calcium oxide-magnesium oxide-iron oxide(FeO)-iron oxide (Fe_2O_3)-alumina-silica-titania-water-carbon dioxide. *J. Petrol.* 1988, **29**, 445–522.
19. Gutt, W., *Nature* 1965, **207**, 184–185.
20. Schlaudt, C. M. and Roy, D. M., The Join Ca_2SiO_4–$CaMgSiO_4$. *J. Am. Ceram. Soc.* 1966, **49**, 430–432.
21. Sharp, Z. D., Essene, E. J., Anovitz, L. M., Metz, G. W., Westrum, J. E. F., Hemingway, B. S. *et al.*, The heat capacity of a natural monticellite and phase equilibria in the system CaO–MgO–SiO_2–CO_2. *Geochim. Cosmochim. Acta.* 1986, **50**, 1475–1484.
22. Yoder, Jr. H. S., Akermanite and related melilite-bearing assemblages. *Carnegie Inst. Washington Yearbook* 1968, 471–483.
23. Osborn, E. F., The compound merwinite and its stability relations within the system CaO–MgO–SiO_2 (preliminary report). *J. Am. Ceram. Soc.* 1943, **26**, 321–332.
24. Ricker, R. W. and Osborn, E. F., Additional phase-equilibrium data for the system CaO–MgO–SiO_2. *J. Am. Ceram. Soc.* 1954, **37**, 133–139.
25. Yang, H. Y., New data on fosterite and monticellite solid solutions. *Am. Miner.* 1973, **58**, 343–345.
26. Biggar, G. M. and O'Hara, M. J., Monticellite and fosterite crystalline solution. *J. Am. Ceram. Soc.* 1969, **52**, 249–252.
27. Adams, G. E. and Bishop, C. F., An experimental investigation of thermodynamic mixing properties and unit-cell parameters of forsterite–monticellite solid solution. *Am. Miner.* 1985, **70**, 714–722.
28. Hatfield, T., Richmond, C., Ford, W. F. and White, J., Compatibility relationships between the periclase and silicate phases in magnesite refractories at high temperatures. *Trans. Br. Ceram. Soc*. 1970, **69**, 53–58.

29. Warner, R. D. and Luth, W. C., Two-phase data for the join monticellite ($CaMgSiO_4$)–Forsterite (Mg_2SiO_4): experimental results and numerical analysis. *Am. Miner.* 1973, **58**, 998–1008.
30. Brousse, C., Newton, R. C. and Kleppa, O. J., Enthalpy of formation of forsterite, enstatite, akermanite, monticellite and merwinite at 1073 K determined by alkali borate solution calorimetry. *Geochim. Cosmochim. Acta* 1984, **48**, 1081–1088.
31. Ferguson, J. B. and Merwin, H. E., The ternary system CaO–MgO–SiO_2. *Am. J. Sci.* 1919, **284**(4th Ser), 81–123.
32. Biggar, G. M. and O'Hara, M. J., Retrograde solubility of periclase, forsterite, and dicalcium silicate. *J. Am. Ceram. Soc.* 1970, **53**, 538–540.
33. Roy, D. M., Subsolidus data for the join Ca_2SiO_4–$CaMgSiO_4$ and the stability of merwinite. *Miner. Mag. J. Miner. Sci.* 1956, **31**, 187–194.
34. Kosa, L., Adamkovicova, K. and Proks, I., *Silikaty Prague* 1985, **25**, 199–206.
35. http://www.factsage.com, 2004.
36. Bowen, N. L., The ternary system: diopside–fosterite–silica. *Am. J. Sci.* 1914, **38**, 207–264.
37. Boyd, F. R. and Schairer, J. F., The System $MgSiO_3$–$CaMgSi_2O_6$. *J. Petrol.* 1964, **5**, 275–309.
38. Kushiro, I., Determination of liquidus relations in synthetic silicate systems with electron probe analysis: the system fosterite-diopside-silica at 1 atmosphere. *Am. Miner.* 1972, **57**, 1260–1270.
39. Schairer, J. F. and Yoder, Jr. H. S., The system diopside–enstatite–silica. *Carnegie Inst. Washington, Yearbook* 1962, **61**, 75–82.
40. Kushiro, I. and Schairer, J. F., New data on the system diopside-fosterite-silica. *Carnegie Inst. Washington, Yearbook* 1963, **62**, 95–103.
41. Yang, H. Y., *Am. J. Sci.* 1973, **273**, 488–497.
42. Longhi, J., In *Proceedings of ninth Lunar Planetary Science Conference*, 1978, pp. 285–306.
43. Longhi, J. and Boudreau, A. E., The orthoenstatite liquidus field in the system fosterite-diopside-silica at one atmosphere. *Am. Miner.* 1980, **65**, 563–573.
44. Jenner, G. A. and Green, D. H., *Miner. Mag.* 1983, **47**, 153–160.
45. Biggar, G. M., Calcium-poor pyroxene: phase relations in the system CaO–MgO-Al_2O_3–SiO_2. *Miner. Mag.* 1985, **49**, 49–58.
46. Carlson, W. D., Subsolidus phase equilibria on the forsterite-saturated join $Mg_2Si_2O_6$–$CaMgSi_2O_6$ at atmospheric pressure. *Am. Miner.* 1988, **73**, 232–241.
47. Newton, R. C., Charlu, T. V., Andreson, P. A. M. and Kleppa, O. J., Thermochemistry of synthetic clinopyroxenes on the join $CaMgSi_2O_6$–$Mg_2Si_2O_6$. *Geochim. Cosmochim. Acta* 1979, **41**, 55–60.
48. Perrotta, A. J. and Stephenson, D. A., Clinoenstatite: high-low inversion. *Science* 1965, **148**, 1090–1091.
49. Smith, J. V., Magnesium pyroxenes at high temperature: inversion in clinoenstatite. *Nature* 1969, **222**, 256–257.
50. Shearer, J. A. and Kleppa, O. J., Enthalpies of formation of spinel ($MgAl_2O_4$), pyroxene ($MgSiO_3$), olivine (Mg_2SiO_4), kyanite (Al_2SiO_5), and sillimanite (Al_2SiO_5) by oxide melt solution calorimetry. *J. Inorg. Nucl. Chem.* 1973, **35**, 1073–1078.
51. Allen, T., White, F. P., Wright, F. E. and Larsen, E. S., *Am. J. Sci.* 1909, **27**, 1–47.
52. Schairer, J. F. and Bowen, N. L., The binary system $CaSiO_3$–diopside and the relations between casio$_3$ and akermanite. *Am. J. Sci.* 1942, **240**, 725–742.
53. Osborn, E. F., The System $CaSiO_3$-Diopside-Anorthite. *Am. J. Sci.* 1942, **240**, 751–788.
54. Tarina, I., Navrotsky, A. and Gan, H., Direct calorimetric measurement of enthalpies in diopside–anorthite–wollastonite melts at 1773 K. *Geochim. Cosmochim. Acta* 1994, **58**, 3665–3673.
55. De Yoreo, J. J., Lange, R. A. and Navrotsky, A., Scanning calorimetric determinations of the heat contents of diopside-rich systems during melting and crystallization. *Geochim. Cosmochim. Acta* 1995, **59**, 2701–2707.
56. Navrotsky, A., Ziegler, D., Oestrike, R. and Maniar, P., Calorimetry of silicate melts at 1773 K: measurement of enthalpies of fusion and of mixing in the systems diopside-anorthite-albite and anorthite-fosterite. *Contrib. Miner. Petrol.* 1989, **101**, 122–130.
57. Ziegler, D. and Navrotsky, A., Direct measurement of the enthalpy of fusion of diopside. *Geochim. Cosmochim. Acta* 1986, **50**, 2461–2466.
58. Lange, R. A., Yoreo, J. J. D. and Navrotsky, A., Scanning calorimetric measurement of heat capacity during incongruent melting of diopside. *Am. Miner.* 1991, **76**, 904–912.
59. Stebbins, J. F., Carmichael, I. S. E. and Weill, D. E., The high temperature liquid and glass heat contents and the heats of fusion of diopside, albite, sanidine and nepheline. *Am. Miner.* 1983, **68**, 717–730.
60. Richet, P. and Bottinga, Y., Anorthite, andesine, wollastonite, diopside, cordierite and pyrope: thermodynamics of melting, glass transitions, and properties of the amorphous phases. *Earth. Planet. Sci. Lett.* 1984, **67**, 415–432.
61. Navrotsky, A., Ziegler, D., Oestrike, R. and Maniar, P., Calorimetry of silicate melts at 1773 K: measurement of enthalpies of fusion and of mixing in the systems diopside–anorthite–albite and anorthite–fosterite. *Contrib. Miner. Petrol.* 1989, **101**, 122–130.
62. Schairer, J. F. and Kushiro, I., *Carnegie Inst. Washington, Yearbook* 1963–1964, **63**, 130–132.
63. Kushiro, I. and Schairer, J. F., *The Join Diopside-Alkermanite*. Carnegie Institute of Washington, 1964, 132–133.
64. Valley, J. W. and Essene, E. J., *Contrib. Miner. Petrol.* 1980, **74**, 143–152.
65. Schairer, J. F. and Bowen, N. L., *Am. J. Sci.* 1942, **240**, 725–742.
66. Yoder, Jr. H.S., *Fostschr. Miner.* 1973, **50**, 140–173.
67. Yoder, Jr. H.S., *Phys. Chem. Earth* 1975, **9**, 883–894.
68. Proks, I., Eliasova, M. and Kosa, L., The heat of fusion of akermanite. *Silikaty* 1977, **1**, 3–9.
69. Adamkovicova, K., Nerad, I., Kosa, L., Liska, M., Strecko, J. and Proks, I., Enthalpic analysis of melts in the $Ca_2MgSi_2O_7$–$CaSiO_3$ system. *Chem. Geol.* 1996, **128**, 107–112.
70. Nerad, I., Adamkovicova, K. and Kosa, L. S. J. P. I., Differential and integral enthalpies of solution of akermanite and pseudo-wollastonite in the melt of the system $Ca_2MgSi_2O_7$–$CaSiO_3$. Isoplethal enthalpies in this system. *Thermochim. Acta* 1996, **276**, 49–55.
71. Spencer, D. R., Beamond, T. W. and Coleman, D. S., The solubility of CaO in MgO and its effect on the CaO–MgO–SiO_2 system at 1800 °C. *Trans. Br. Ceram. Soc.* 1970, **70**, 31–33.
72. Sakai, H. and Suito, H., Liquid phase boundaries at 1873 K in the ternary CaO–Al_2O_3–MO_x(MO_x: MgO, ZrO_2) and CaO–SiO_2–MO_x(MO_x: TiO_2, MgO, Al_2O_3) systems. *ISIJ Int.* 1996, **34**, 138–142.
73. Greig, J. W., Immiscibility in silicate melts. Part I. *Am. J. Sci.* 1927, **13**(5th Ser), 1–44.
74. Kirschen, M. and DeCapitani, C., Experimental determination and computation of the liquid miscibility gap in the system CaO–MgO–SiO_2-TiO_2. *J. Phase Equilib.* 1999, **20**, 593–611.
75. Harker, R. J. and Tuttle, O. F., *Am. J. Sci.* 1956, **254**, 468–478.
76. Walter, L. S., *Am. J. Sci.* 1963, **261**, 488–500.
77. Rein, R. H. and Chipman, J., Activities in the liquide solution SiO_2–CaO–MgO–Al_2O_3 at 1600 °C. *TMS-AIME* 1965, **233**, 415–425.
78. Morita, K., Kume, K. and Sano, N., A newly developed method for determining SiO_2 activity of the silicate slags equilibrated with molten silicon alloys. *ISIJ Int.* 2000, **40**, 554–560.
79. Henderson, D. and Taylor, J., Thermodynamic properties in the CaO–MgO–SiO_2 and MgO–Al_2O_3–SiO_2 systems. *J. Iron Steel Inst.* 1966, 39–43.
80. Kalyanram, M. R., MacFarlane, T. G. and Bell, H., The activity of calcium oxide in slags in the system CaO–MgO–SiO_2, CaO–Al_2O_3–SiO_2, and CaO–MgO-Al_2O_3–SiO_2 at 1500 °C. *J. Iron Steel Inst.* 1960, **58–64**, 195.
81. Sawamura, K., Activity of lime in blast-furnace type slag. *Tetsu-to-Hagane Overseas* 1962, **2**, 219–225.